The Optimization of Golgi-Cox Staining in Parallel with Immunofluorescence to Colocalize the Adhesion Protein, N-Cadherin, to Developing Synapses.

By Victoria Frank

December 2024

Director of Thesis: Karen Litwa
Major Department: Anatomy and Cell Biology

Numerous neurodevelopmental disorders, including Autism Spectrum Disorders (ASD), exhibit altered synapse formation. Post-mortem brain samples from idiopathic cases of ASD exhibit increased numbers of dendritic spines, which are the primary site of excitatory synapse formation. Excitatory synapses facilitate action potential formation, underlying cognitive functions such as learning and memory formation. Excitatory synapses develop in stages: synapse formation begins when post-synaptic spine precursors adhere to a pre-synaptic axon partner. As synapses mature, dendritic spines undergo a morphological transition from filopodia-like spine precursors to mushroom-shaped dendritic spines. These morphological changes increase the surface area adjacent to the axon partner, as well as the number of neurotransmitter receptors, thereby increasing the likelihood of action potential propagation. We are interested in the mechanisms of synapse formation, maturation, and maintenance. While there is considerable research on experience-dependent synapse maturation after birth, we lack understanding of the molecular mechanisms that initiate synapse formation and how these mechanisms are altered by ASD-associated genetic mutations and/or

environmental factors. To address how synapse adherence occurs, we developed techniques to visualize association of the known synaptic adhesion molecule, N-Cadherin, with developing synapses. In this study we will be presenting the process of optimizing Golgi-Cox staining in embryonic mouse brain tissue to visualize post-synaptic dendritic spine morphology and using immunofluorescence in mouse brains to study N-Cadherin's association with developing synapses. Our hypothesis stated that as synapse development progresses there will be an increase in N-Cadherin localized to synapses. Using these techniques, we saw trends which suggest that as the brain develops there will be an increase in the density of N-Cadherin positive synapses over time. Limitations of this study though prevented the acceptation or rejection of our hypothesis, instead it was inconclusive. The association we observed for the increase of N-Cadherin positive synapses over time, suggests a role for N-Cadherin in synapse stabilization/maturation. Further, significant differences were observed in that N-Cadherin positive synapses were larger than the negative N-Cadherin synapses on average. This supports the postulation that N-Cadherin promotes excitatory synapse maturation. Future research will use knockdown approaches to examine the role of N-Cadherin at distinct stages of synapse formation in neuronal cell cultures.

The Optimization of Golgi-Cox Staining in Parallel with Immunofluorescence to Colocalize the Adhesion Protein, N-Cadherin, to Developing Synapses.

A Thesis

Presented to the Faculty of the Department of Anatomy and Cell Biology

East Carolina University

In Partial Fulfillment of the Requirements for the Degree

Master of Biomedical Sciences

By

Victoria Elizabeth~Ray Frank

December 2024

Director of Thesis: Karen Litwa, Ph.D.

Thesis Committee Members:

Alessandro Didonna, Ph.D.

Dr. Stefan Clemens, Ph.D.

Ken Soderstrom, Ph.D.

ACKNOWLEDGEMENTS

There are many whom I would like to thank, starting with Dr. Litwa for taking me into her lab and being such a great Principal Investigator, for dealing with numerous troubles with the utmost patience and understanding. I would also like to thank Michelle Cobb for always being there to answer my questions and to provide help, you are what keep this lab running smoothly. Thank you to Riley Bessetti for allowing me to annoy you with questions and for all the help you have given me as well. I would also greatly like to thank Emma Gilbert because without her this project wouldn't be possible, and also Geyer lab for allowing Emma to help me and provide materials necessary. Many thanks for the invaluable help to my committee members, Dr. Soderstrom, Dr. Clemens, and Dr. DiDonna, for helping sort out my thesis as well as providing me equipment necessary for my project. I would like to give thanks as well to Joani Zary for letting me continuously use her time and equipment to keep my project moving forward, our lovely chats kept me sane. Lastly, I would also like to acknowledge that this work was supported by the National Science Foundation through CAREER award number 2144912 to Dr. Litwa. The content is solely the responsibility of the authors and does not necessarily represent the official views of the National Science Foundation.

TABLE OF CONTENTS

LIST OF FIGURES:

LIST OF SYMBOLS AND ABBREVIATIONS

AMPA	-α-amino-3-hydroxy-5-methyl-4-isoxazolepropionic acid
ASD	-Autism Spectrum Disorder
CA1	-Hippocampal cornu ammonis
CDC	-Center for Disease Control & Prevention
DIV	-Days in vitro
E18.5	-Embryonic Day 18.5
FMRP	-Fragile X mental retardation protein
IF	-Immunofluorescence
KO	-Knockout
LED	-Light Emitting Diode
LTP	-Long Term Potentiation
mEPSC	-miniature Excitatory Postsynaptic Current
MAP2	-Microtubule associated protein 2
M.O.M	-Mouse on Mouse
mRNA	-Messenger RNA
NLG	-Neuroligin
NLG1	-Neuroligin 1
NLG2	-Neuroligin 2
NLG3	-Neuroligin 3
NLG4	-Neuroligin 4
NMDA	-N-methyl-D-aspartate
PCR	-Polymerase chain reaction

PBS	-Phosphate Buffer Solution
PND	-Post natal day
WT	-Wild type

Introduction

Autism Spectrum Disorder

Autism Spectrum Disorder (ASD) is a neurodevelopmental disorder that affects one in thirty-six children according to the most recent data from the CDC[1]. ASD is the fastest growing developmental disability, witnessing a meteoric rise since its first diagnosis in the 1940s by Leo Kanner, at which time only four in ten thousand children were thought to be affected[2]. Many factors contribute to the recent increase in ASD prevalence. One factor is an expansion of the diagnostic criteria for ASD within the past decade, leading to more patients being identified[3,4]. The current Diagnostic Statistical Manual for Mental Disorders (DSM-V) diagnoses ASD by identification of persistent deficits in social communication and social interactions, and the presence of restrictive and repetitive patterns of behaviors or interests must also be observed over time[5]. These diagnostic criterium are often evident in early development, and the American Association of Pediatrics recommends screening for all children for ASD around the age of 2[5,6].

As a spectrum disorder, many environmental and genetic factors contribute to the development of autism. Environmental factors possibly affecting the development of ASD include traumatic pregnancies and exposure to carcinogenic substances. Current research shows that disturbances in pregnancy caused by bleeding, gestational diabetes, intrauterine infections, or medications the mother takes can contribute as risk factors for the child developing ASD[7]. One medication called valproic acid, which is now banned for use in pregnant women in most countries, increased ASD risk in human offspring and is used to model autism-like phenotypes in both cell cultures and mouse

models[8]. Having a high risk pregnancy or complications during birth can also increase the risk of development of ASD[7].

In addition to these environmental factors, genome-wide association studies of ASD-associated genetic alterations implicate specific biological processes in ASD pathogenesis. For example, many ASD-associated genes converge on the regulation of synapse development and function[4,7,9,10]. Some of these synaptic ASD-associated genes encode for synaptic adhesion proteins such as *NLG1* (Neuroligin-1), *NLG3* (Neuroligin-3), *NRXN1* (Neurexin-1) and *CADM1* (encoding for the protein SynCAM1)[7,11]. Others impact synaptic scaffolding proteins, such as *SHANK3* or synapse regulatory proteins like *PCDH8* (Protocadherin-8), and many more[7,12]. Some of

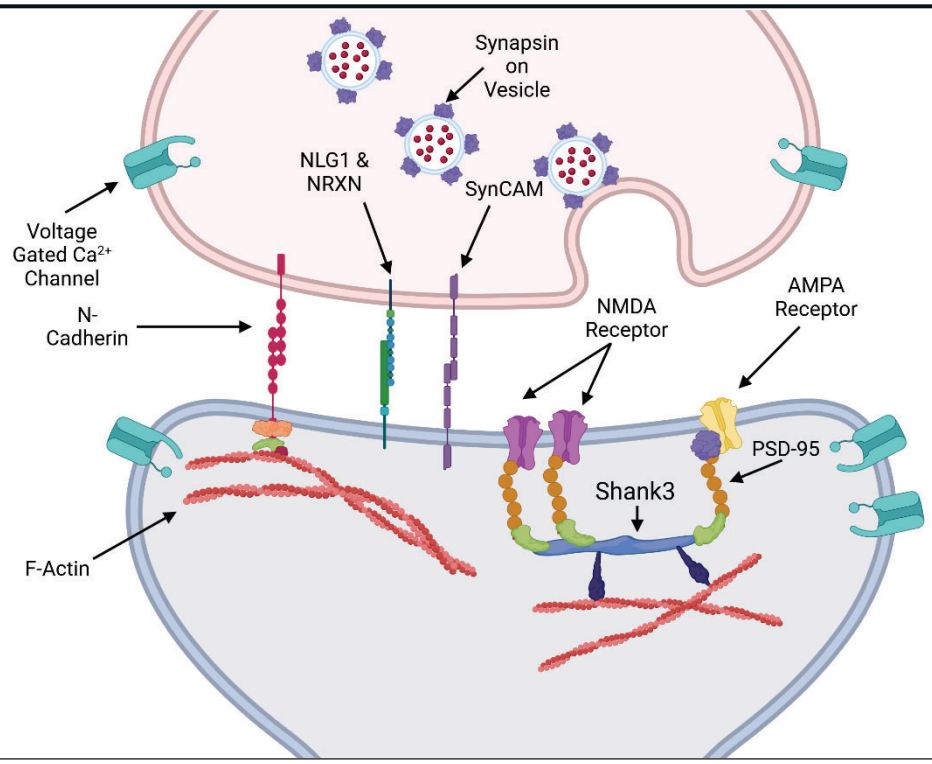

Figure 1, Illustration of Proteins in Synapses: A representation of the components and proteins in the synapse. Some of the genes encoding for these proteins are known to be risk factors for developing ASD if mutated. Created in Biorender.com.

these proteins are illustrated in Figure 1. Consistent with these genetic mutations, synaptic alterations are a hallmark of ASD.

Synapses are sites of information transfer in neural circuits, which we will discuss more fully later in the introduction. Specifically, excitatory synapses facilitate action potential propagation[13]. The majority of excitatory synapses form on specialized projections, known as dendritic spines[13]. In ASD post-mortem brains, these dendritic spines can be used to assess synaptic alterations. Studies of idiopathic autism cases reveal increased dendritic spines in cortical brain regions[14]. Idiopathic cases of ASD are different than syndromic cases as they do not have a known genetic cause or history in the family to account for the development of the disorder. The increased density of dendritic spines then forms greater numbers of synapses when they connect to their pre-synaptic partner, the axon terminal. This change in synapse number affects the individual by altering the neural circuits in the brain, producing the deficits in social interaction and the increase in repetitive behaviors seen in ASD[15]. However, the majority of these post-mortem studies focus on childhood and early adolescence[14]. Thus, in our present research, we seek to optimize techniques to assess the morphological differences and molecular mechanisms across the lifespan, including understudied periods of synapse formation early fetal/infant stages to later geriatric stages to assess aging-related synapse loss. With the broadening of the ASD diagnostic criteria and the rapid rise in prevalence over the past 20 years, such samples are becoming available for study. Additionally, our lab generates human cortical brain which model fetal synaptogenesis[16,17]. The goal of the current research is to optimize techniques to assess synaptic changes across lifespan in order to assess how ASD-associated

genetic and environmental factors impact this trajectory. Ultimately, this research will help to identify windows of opportunity for therapeutic intervention, which is particularly needed with increased rates of ASD diagnosis.

Around 30% of those diagnosed with ASD receive medical care for behavioral or psychiatric issues[10]. The current estimation of medical care costs across the lifetime of individuals diagnosed with ASD is 3.6million US dollars[18]. New evidence from a recent study highlights that those diagnosed with ASD have a 4.04% prevalence of developing early onset Alzheimer's disease compared to the neurotypical prevalence of 0.97%[18]. This high prevalence is even greater when intellectual disorders are comorbid with ASD[18]. The described association between the two developmental disorders is perplexing, considering one of the phenotypes of ASD is an increase in dendritic spine density[14,19]. An increase in dendritic spines would have thought to be protective against developing Alzheimer's Disease, as with Alzheimer's there is a loss of dendritic spines

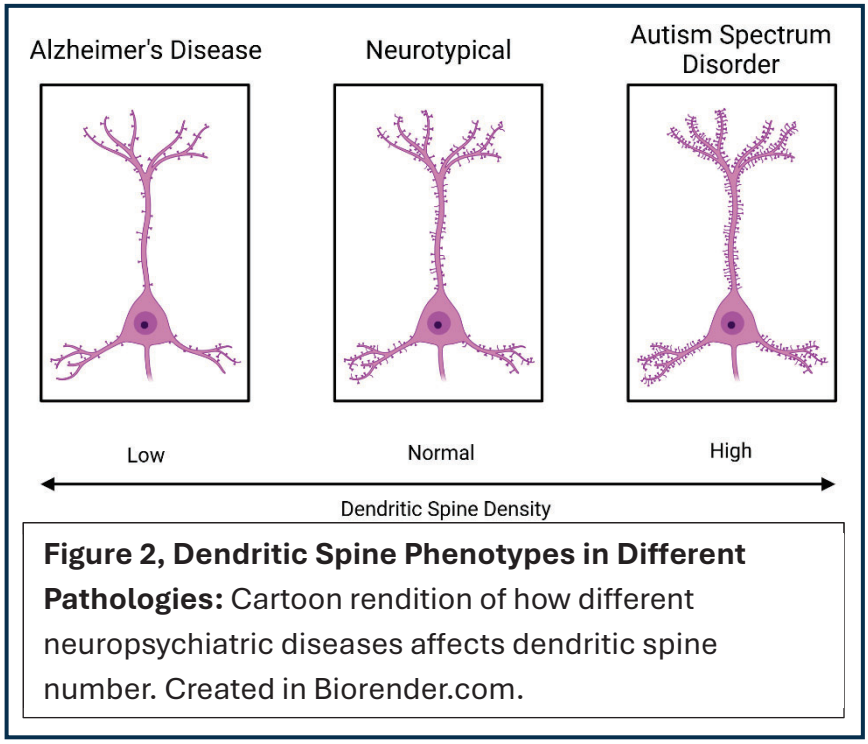

Figure 2, Dendritic Spine Phenotypes in Different Pathologies: Cartoon rendition of how different neuropsychiatric diseases affects dendritic spine number. Created in Biorender.com.

over time, but this new correlational data shows the need to explore the connections between the two neuropsychiatric disorders[18,20–24]. There is limited information on synapses in the brain of ASD individuals across all stages of human life, as most data acquired from post-mortem brain tissue is acquired from those who died in adolescence[14]. This adds emphasis to our goal to optimize techniques to study synaptic changes across the lifespan, ultimately including post-mortem geriatric ASD brain samples which are now available. In order to fully understand the complexity of ASD we need to first fully explore how synapses in the central nervous system (CNS) function, their role in the CNS, and their individual components.

Synapses in the Central Nervous System

Synapses are the connections between two neurons that allow for communication via chemical signaling that initiates an electrical impulse called an action potential. Connections between neurons can be excitatory or inhibitory, based on the receptors they express[13]. Excitatory synapses are responsible for initiating an action potential formation. Action potentials propagate information throughout neural circuits and will be explained more later, while inhibitory synapses decrease the likelihood that an action potential will occur. Excitatory synapses are formed on specialized post-synaptic dendritic protrusions called dendritic spines, which can be easily identified through Golgi staining, as opposed to inhibitory synapses which form along the dendrite and cannot be visually discerned by the staining of the neuronal architecture[13]. The dendritic spine head of the excitatory synapse contains an electron-dense post-synaptic density (PSD) area. The PSD is comprised of specialized proteins such as PSD-95, which can be used as an excitatory post-synaptic marker in immunofluorescence (IF).

The post-synaptic spines are one half of the synapse, the other being the pre-synaptic compartment known as the axon terminal. The post-synaptic spines are one half of the synapse, the other being the pre-synaptic compartment known as the axon terminal, where neurotransmitters are packaged into the synaptic vesicles. Thus, the pre-synaptic compartment of excitatory synapses can be identified by immunostaining for synaptic vesicle-associated proteins. For example, in our present study we will identify pre-synaptic axon terminals by immunostaining for the synaptic vesicle-associated protein, synapsin. Synapsin tethers synaptic vesicles to the actin cytoskeleton regulates vesicle

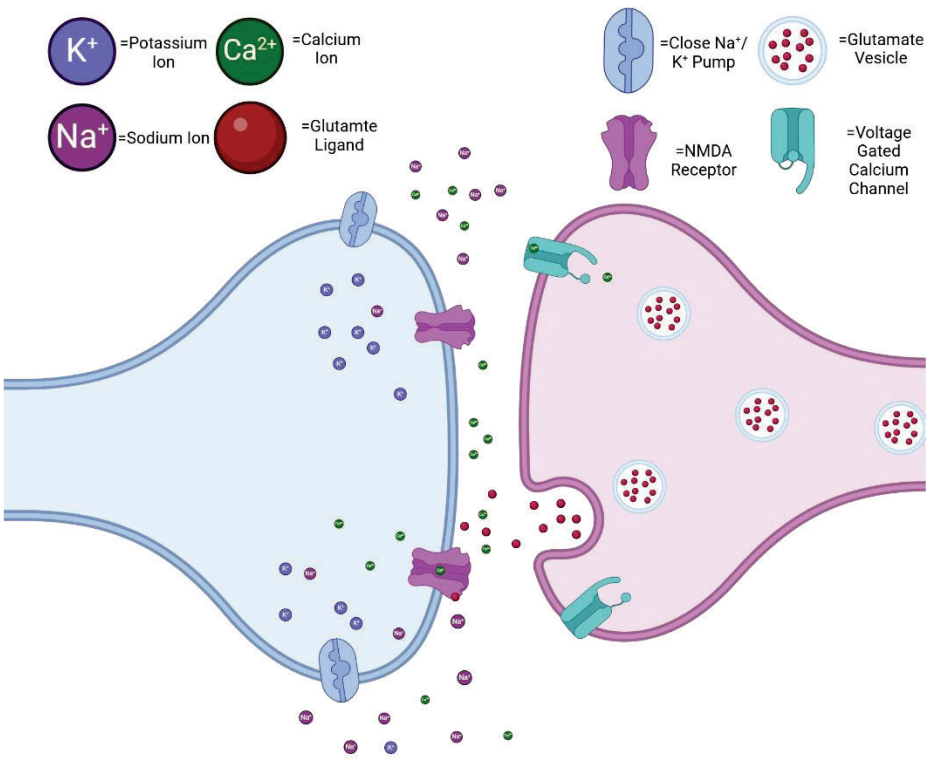

Figure 3, Representation of an Excitatory Synapse: Cartoon rendition of a synapse, illustrating the pre and post synaptic membrane. The pre-synaptic membrane has vesicles releasing glutamate into the synaptic cleft. This allows Ca^{2+} to enter through the NMDA receptor and potentially initiate the opening of the voltage gated calcium channels to start an action potential. Created in Biorender.com

fusion to the pre-synaptic membrane[25]. Upon fusion neurotransmitters, such as glutamate, are released into the synaptic cleft where they can bind to neurotransmitter receptors on the adjacent post-synaptic surface[26]. Glutamate is an excitatory neurotransmitter and binding to ionotropic glutamate receptors, such as AMPAR or NMDAR, leads to membrane depolarization (Fig. 3). With sufficient membrane depolarization (from -70mV to -50mV), an action potential will be generated.

Action potentials are the driving force in neuron function; they transfer information across neural network[25]. The neuron sums the membrane potential across the receptive field of synapses, both inhibitory and excitatory. At glutamatergic excitatory synapses, the influx of Na^+ ions across the plasma membrane results in membrane depolarization, while at inhibitory synapses, Cl- influx results in membrane hyperpolarization[25]. The summation of the membrane potential at the axon hillock will determine whether the membrane threshold is achieved. If the influx of ions changes the resting membrane potential of -70mV to the threshold of activation membrane potential of -50mV, an action potential will occur. If the threshold is not met there will be no event generated[25]. After the activation threshold is met the cell further depolarizes to a peak of +50mV from an influx of Na^+ ions from the voltage gated Na^+ channels[25]. These channels only open after a certain voltage requirement is met. At the peak of depolarization of the action potential, the cell repolarizes through an efflux of K^+ causing a halt to the movement of Na^+ from the voltage gated channels closing, allowing the membrane to return to baseline[25]. The process described is known as repolarization; it is the last stage in the generation and propagation of action potentials[25]. It is this series

of events that allows information to be carried through connected neuronal networks in the brain and ensure its proper function.

The process of synapse formation represents the culmination of neuronal differentiation, axonal guidance via chemical cues, neural migration, and dendritic spine morphogenesis[32,34]. In humans, synapse formation begins in mid-fetal gestation and peaks in early childhood[31]. Once developed, neural activity within neural networks affects synapses by either strengthening or weakening the connection between the pre- and post-synaptic membranes[35]. With repeated stimulation, strengthening increases the post-synaptic surface area, the number of glutamate receptors increases adjacent to the axon terminal[26]. The increased glutamate receptors increase the likelihood that that membrane threshold for action potential formation will occur. Synaptic strengthening underlies learning and memory formation[26]. Strengthening of neural connections is crucial for creating efficient neural pathways. By contrast, pruning of unused synapses occurs through dendritic spine reabsorption or microglial phagocytosis[27,28].. This allows for pathways to become more efficient and create sophisticated neural networks[27]. Abnormalities in the formation and pruning of synapses during critical developmental periods are associated with several neurodevelopmental and neuropsychiatric disorders[10,14,20–22,24,28,29]. Knowing that alterations in synapse development and maintenance can cause drastic abnormalities creates a fervor to understand synaptogenesis. In order to better understand these disease-associated synaptic alterations, we will first describe how synapses, and specifically dendritic spines, typically develop.

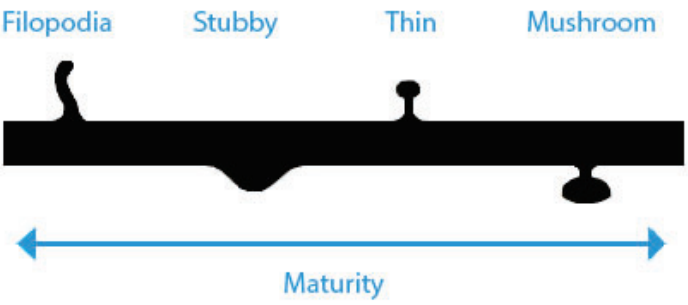

Figure 4, Different Dendritic Spine Morphologies: Cartoon rendition of the different dendritic spine morphologies. Original image created in Photoshop.

As stated previously, synaptogenesis involves the creation of synapses in the brain as it develops. One specific type of synapse created is the axo-dendritic connection. In Vaughn's theory of synaptogenesis, the filopodia spines are the post-synaptic component responsible for initiating the first contact with axons to create immature synaptic junctions[30]. The filopodia spine extends outwards, as its stalk is far longer than the other morphologies, to initiate and create contact with the extending axon growth cone[27,30,31]. This is in accordance with recent data showing that early developing dendrite branches have more dynamic filopodia that transition into the stable thin or mushroom shaped spines as they mature[27,31]. Figure 4 provides a visual depiction of the different morphologies of dendritic spines. Thin spines are named after their thin protruding stalk from the dendrite, accompanied by a round bulbous head; whereas, stubby spines are short with almost no stalk that creates a rounded hilltop appearance[27,32]. The mushroom spines have a shorter slender stalk when compared to the thin morphology and also have a large with a flat top that appears similar to a mushroom[27,32]. The last morphology is the filopodia spine which can be compared to thin protruding fingers[27]. The stubby and filopodia spines are associated with immature

development and the thin and mushroom spines with mature development in synapses[33]. The maturity of a spine is based on its ability to create a strong connection with its pre-synaptic partner as well as the complexity of its internal components. The mature spines have greater connective strength versus the immature may have a weak connection or no connection yet to its pre-synaptic partner[22,30]. Mature synapses are associated with mushroom and thin dendritic spines due to the increased surface area the bulbous head provides[27]. The larger surface area allows for greater quantities of receptors to be expressed in the post-synaptic membrane. This aids in increasing the frequency of action potentials as there will be greater rates of excitatory receptor expression to initiate their generation by increasing the likelihood of depolarizing the membrane potential to reach the threshold of activation[25,34]. In order to support the greater quantity of receptors, more scaffolding proteins must also be expressed in the PSD to help stabilize the receptors on the surface and connect them to their intracellular effectors[34].

The PSD is contained inside the bulbous head of the mushroom spine. The top area of the PSD includes adhesion proteins which allow for stable connections to form with the pre-synaptic partner or axon terminal. The PSD also contains scaffolding proteins whose purpose is to stabilize receptors in the surface membrane and connect them to the receptor's intracellular effectors[34]. Post-synaptic density protein 95 (PSD-95) is one such protein that clusters under glutamate receptors to stabilize them[26]. It also interacts with the Stargazin protein, a regulatory protein of α-Amino-3-Hydroxy-5-Methyl-4-Isoxazolepropionic Acid (AMPA) receptors, to help anchor and stabilize the AMPA receptors to the post-synaptic membrane[34]. The Shank family is another group of

scaffolding proteins where one of the genes encoding for Shank3 has implications in ASD when mutated[34–36]. One function of Shank3 is to help with repolarization of the neuron by binding to voltage activated calcium channels and the anchoring of glutamate receptors to the post-synaptic surface membrane[34,36]. The PSD also houses structural proteins such as actin and microtubule associated protein 2 (MAP2)[34,37,38]. Actin is predominantly found in dendritic spines and has been shown to be involved in neural plasticity and potentially involved in transitioning immature spines into the mature morphologies[37,39–41]. Microtubules are also found in the PSD but are not present in the same permanent capacity as actin or MAP2. Instead, microtubules transiently will enter the PSD[37,42]. In recent studies that utilized live cell imaging, microtubules were shown to help maintain dendritic spine structure[37,42]. These scaffolding proteins all have greater expression in the mature mushroom morphology of dendrites and are now being shown to be involved in dendritic spine formation and neural plasticity[26,34–37,39–45]. Neural plasticity refers to the process in the brain where neural connections are altered in response to stimuli[46]. Part of the process for neural plasticity is long term potentiation (LTP), and both are connected with dendritic spines maturing. LTP occurs when neural activity strengthens a connection and enhances learning through the initiation of events leading to increased receptor and protein expression[45]. LTP is initiated through the binding of glutamate to N-Methyl-D-Aspartate receptors (NMDA), triggering a cascade response, which enhances AMPA receptor expression[34,45]. The increase in the surface expression of ionotropic glutamate receptors increases the likelihood that the synapse will reach the depolarized threshold necessary to initiate an action potential. In addition

to ionotropic glutamate receptors, expression of associated scaffolding proteins also increases during the process of synaptic strengthening[34].

In the present study, we have optimized a methodology to examine temporal changes in proteins associated with developing synapses. Our goal was to determine what adhesion proteins localize to synapses during their initial formation and strengthening. Future studies will be conducted to address whether these molecules are necessary for the initiation of synapse formation. To conduct the optimizations, we first used Golgi-Cox staining to examine the morphology of dendritic spines spanning mouse embryonic day 18.5 (E18.5, synapse initiation), post-natal day 6-7 (PND6-7, synapse stabilization), and post-natal day 17-20 (PND17-20, synapse maturation). This study examines how the excitatory synapse adhesion molecule, N-Cadherin, localizes to synapses at these different developmental stages. We will briefly review the known roles of a few adhesion molecules and their association with neuropsychiatric disorders. Also discussed will be the what is currently known about the role synaptic protein N-Cadherin has in both dendritic morphogenesis and synaptogenesis.

The Role of Adhesion Proteins in Synapses

Adhesion proteins stabilize newly formed connections during synaptogenesis and to help facilitate dendritic spine morphogenesis during synapse maturation[33,44,47–53]. Not surprisingly, variations in the genes expressing for synaptic adhesion, such as genes containing copy number variants, are often associated with ASD[7,54]. One group of genes that are known to be associated with the development of ASD, if perturbed, are those encoding for synaptic adhesion proteins[7,54]. Of these genes, some are found to express proteins involved in the cadherin-catenin complex[7,55,56]. This complex contains N-

Cadherin, an adhesion protein expressed in both the pre- and post-synaptic membranes of synapses[7,12,57]. Pcdh8 and the various catenins help to regulate the expression and function of N-Cadherin have been identified through genome-wide association studies to be linked to ASD if their associated genes are altered[7,12,57]. Current knowledge also states that N-Cadherin has a role in the initial stages of synaptogenesis, though the underlying molecular mechanisms involved are unknown[49,58–60]. We are interested in investigating N-Cadherin and the relationship it has in the beginning stages of synaptogenesis, as well the role N-Cadherin has in the overall lifetime of ASD and its potential connection to the development of Alzheimer's Disease later in life. In this section we will be discussing the cadherin-catenin complex and their roles in synapse formation & maturation in the neuroepithelium and its connections to ASD.

N-Cadherin is a Type I cadherin family protein that is a homophilic calcium dependent cell adhesion molecule[48,49]. Adheren junctions rely on N-Cadherin to help form bridges between adjoining cells to adhere them together, making it an essential protein for the organization of the neuroepithelium. The neuroepithelium will later develop into the different parts of the central nervous system during human embryonic development[58]. N-Cadherin also participates in axon growth and synapse formation[48,49,58–60] . In Vaughn's theory of excitatory synapse formation the filopodia catches the extending axon and N-Cadherin helps stabilize this connection by creating adhesion between the pre and post-synaptic membranes through homophilic interactions[30,49]. N-Cadherin not only helps to stabilize this connection but it helps in dendritic spine morphogenesis, or the expansion of the dendritic spine head as it matures[48,49]. Togashi et al. 2002 used *in vitro* neuronal cell cultures, and added a

nonfunctional variant of N-Cadherin at days *in vitro* (DIV) 18[49]. Afterwards the shape of the dendrites became abnormal, with a bifurcated head or a filopodia like phenotype[49]. Abnormal dendritic spines hamper synaptic function and plasticity which are necessary for the brain to function properly. Instead, at this stage *in vitro* the spine heads should be in the thin or mushroom morphologies and this was seen in the control neuron cultures[49]. When stained for PSD-95 and synapsin1, there was decreased accumulation of each protein in the dendritic spine head and axon terminal, indicating that nonfunctional N-Cadherin disturbs the support proteins that are necessary for neurotransmission and synapse function[49]. Furthermore Okamura et al. 2005, used real time imaging with immunofluorescence (IF), introduced a W2A mutant of N-Cadherin with negated adhesive function to neuronal cultures to investigate N-Cadherin's role in synapse function and stabilization[48]. The mutant inhibited the lateral expansion of the dendritic spine head, preventing LTP through AMPA receptor activation[48]. These results support Togashi et al.'s conclusion that N-Cadherin is a necessary protein for dendritic spine morphogenesis and synapse function. Although we can observe the connection between N-Cadherin, synapse formation, and maturation; the underlying molecular mechanisms are mechanism is still unknown.

An issue which arises when studying N-Cadherin *in vivo* is when the associated gene is deleted in mice, fatalities occur during the early embryonic stages from heart failure. This led many researchers to create knockouts of proteins that interact with N-Cadherin instead, to form indirect observations of the roles N-Cadherin has in synapse maturation in both *in vivo* and *in vitro*. β-catenin is an intracellular protein which binds to the C-terminal domain of N-Cadherin, serving to connect N-Cadherin to the actin

cytoskeleton (Figure 5). α-catenin and δ-catenin are two other catenins that serve similar functions to β-catenin in the cadherin-catenin complex. A study by Okuda et al. 2007 investigated β-catenin by observing the ramifications of inactivating its associated gene in cultured mouse hippocampal neurons after synaptogenesis on the post-synaptic components by transfecting them after DIV8[61]. The neurons were transfected after DIV8 to avoid perturbation of synaptogenesis during the beginning of cell culture[61]. Neurons that had been transfected with a plasmid at DIV8 to inactivate the β-catenin gene showed thin and elongated dendritic spines, with a drop in the mushroom morphology frequency compared to the control neurons. While the spines heads showed malformations and had altered ratios between the morphologies, there was no overall reduction of the total spine density. Similarly, a study Okuda et al. 2007 also removed β-catenin post-synaptically where the amplitude of the miniature excitatory post-synaptic currents (mEPSCs) was reduced by 25% compared to control neurons[61]. They compared this to the role of N-Cadherin by creating a mutant N-Cadherin with loss of its extra cellular domain and recording mEPSCs with patch clamps. They conclude that the loss of N-Cadherin's extracellular domain resulted in a 30% decrease in mEPSC size, further supporting the role of N-Cadherin and B-catenin in facilitating synapse function[61]. Overall the results of the discussed experiments indicate that the post-synaptic interaction between N-Cadherin and β-catenin are integral for synapse function and dendritic spine morphogenesis[49,61].

In addition to β-catenin, α-catenin and δ-catenin have also been studied for their roles in cateniN-Cadherin complex and in synaptogenesis. Togashi et al. 2002 sought to investigate this complex by designing an experiment that utilized an α-catenin knockout (KO) mouse to observe the effects on the brain structure and on N-Cadherin activity. The neurons formed elongated dendritic spines with considerable variation at DIV10-30[49]. The shape of the dendritic spine head varied significantly more than in control neurons but the overall mean size was not statistically different compared to control

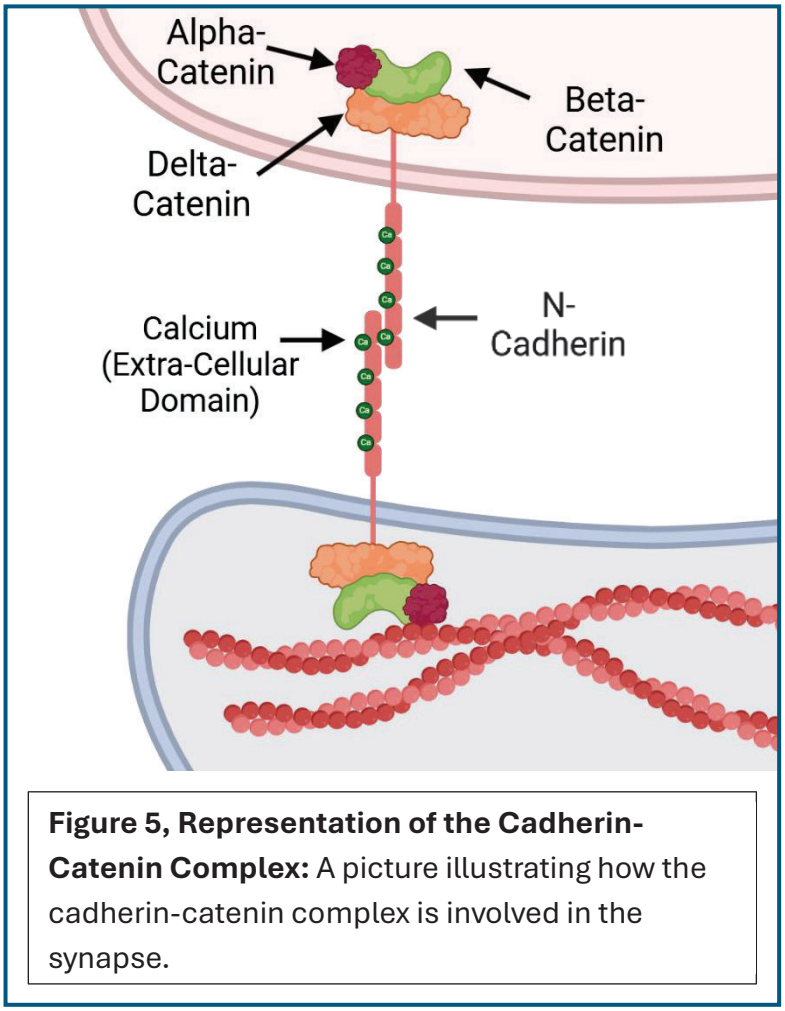

Figure 5, Representation of the Cadherin-Catenin Complex: A picture illustrating how the cadherin-catenin complex is involved in the synapse.

neurons[49]. Deleting the α-catenin and N-Cadherin gene in mice led to early death in mice making it impossible to investigate their effects on mice behavior. However, the δ-

catenin gene has been successfully removed from mice and did not cause death allowing researchers to investigate behavioral changes in mice with altered cadherin-catenin complexes. In Israely et al. 2004, they developed a line of homozygous mutant mice where the δ-catenin gene was targeted for deletion[55]. Spatial memory was tested in both wild-type (WT) and KO mice using the hidden platform Morris Water Maze test[55]. The KO mice were unable to learn where the hidden platform was over the two week learning period[55]. An interesting behavior displayed in the KO mice was floating in the water during testing, which could be congruent with learned helplessness, an indicator of depression[55,62]. In humans, there is high comorbidity between ASD and conditions such as depression and social anxiety[63]. This illuminates an interesting connection between disturbances in the cadherin-catenin complex and ASD. This connection is further strengthened when combined with the knowledge that disturbances in the human gene for δ-catenin, *CTNND2*, is a known risk factor for developing intellectual disabilities which can be comorbid with ASD[56]. Ryu et al. 2019 created a mouse that overexpressed the δ-catenin gene to observe the effects it would have on memory and anxiety[64]. Anxiety can be measured in mice using the elevated plus maze behavioral test and mice overexpressing δ-catenin were placed into this test to observe their behavior[64]. The overexpressing mice stayed longer in the open arms compared to controls, indicating decreased anxiety during testing[64]. Mice prefer closed spaces and it's inferred that that spending more time in open areas is indicative of less anxiety[64]. When their levels of social anxiety was measure in the novel mouse test the overexpressing mice spent more time investigating the novel mouse versus the familiar empty cage when compared to their control counterparts[64]. This result of spending more

time with a novel mouse is indicative of lesser social anxiety as mice generally prefer their familiar environments over investigating new ones[64]. These two studies highlight that perturbing the cadherin-catenin complex can have significant effects on behavior. In summary, the discussed studies highlight the connection between [64]. In summary, the discussed studies highlight the connection between N-Cadherin and its catenin interactors on the development of neural connections and observed behavior.

Yasuda et al. 2007 described the relationship between ASD and N-Cadherin, stating that when N-Cadherin is not properly internalized during synaptic pruning there is an overabundance of dendritic spines[12]. Synaptic pruning is initiated in adolescence after the bulk of synapses form in early childhood. In ASD, it is theorized that when this event is perturbed leading to an overabundance of excitatory connections[12,19,22]. To investigate the theory of perturbed synaptic pruning, a homozygous KO mouse for the Pcdh8 gene was created so neurons could be disassociated and used in neuronal cell cultures[12]. It was observed that the deletion of Pcdh8 led to an increase in dendritic spines compared to the WT cultures and when the KO cultures were transfected with cDNA for Pcdh8 the normal phenotype was recused[12]. This study was able to demonstrate that Pcdh8 interacts with N-Cadherin and it aids in dendritic spine pruning though the internalization of N-Cadherin[12]. Yasuda et al. 2007 supported this by knocking down N-Cadherin in cell culture models, which did decrease the number of dendritic spines[12]. The conclusion reached from these results are that the internalization of N-Cadherin aids in the reabsorption of dendritic spines into the dendrite, thus removing a synapse[12,43]. There is genetic support as well for this theory, as the Pcdh8 gene is a known risk factor for developing ASD when perturbed[7]. The aforementioned

studies in this section implicate N-Cadherin to be an integral protein for synapse formation, stabilization, and maturation. When perturbed, there are serious effects on

Togashi H., et al. 2002	Rat Hippocampal Neurons P0 Mice Brains Mouse Hippocampal Neurons	Extracellular domain deletion in N-cadherin, Alpha-catenin knockout	Malformed Spines, irregular accumulation of Synapsin1. Death in P0 mice, varied spine head size
Okamura K., et al. 2004	Rat Hippocampal Neurons	W2A mutant N-cadherin (No adhesion properties)	Inhibition of lateral head expansion, AMPA mediated LTP inhibited
Okuda T., et al. 2007	Mouse Hippocampal Pyramidal Neurons	Inactive Beta-catenin gene through Cre/lox Extracellular domain deletion in N-cadherin	Thing & elongated spines, mEPSC amplitude decreased. mEPSC size decreased
Israely I., et al. 2004	Delta-catenin Homozygous -/- Mice	Morris Water Maze(MWM) (Hidden platform)	No learning, floating behavior (learned helplessness/depression)
Ryu T., et al. 2019	Thy-1 promoter for Delta-catenin in mice	Novel Object, Three Chamber Test, Elevated Plus Maze	Lower levels of anxiety, lower social anxiety
Yasuda S., et al. 2007	COS7, L929, & HEK293T cell lines, Cultured Rat & Mice Hippocampal neurons	Arcadlin -/- mice derived neurons, N-cadherin knockdown(KD), various cell markers for IF	Increased dendritic spine density, loss of spines in N-cadherin KD. Pcdh8 gene known risk gene

Figure 6, Summary of Studies Investigating N-Cadherin: A summary representation of the discussed studies relating to N-Cadherin or it's interacting

the development and function of neuronal circuits in the brain. A graph depicting all the results of the experiments discussed is shown in Figure 5. From the information described in this section about N-Cadherin's roles within a synapse has inspired us to hypothesize that as synapse development progresses there will be an increase in N-Cadherin localizing to synapses. This will be achieved through the use of immunofluorescence as it is used often to investigate proteins but to investigate the whole neuron and its processes, we will utilize Golgi staining.

THE FUNDAMENTALS OF GOLGI STAINING

Camillo Golgi, an 19th-century Italian scientist, created the Silver Reaction in 1873. This staining technique created a black substance which could bind to neurons to reveal their neuronal architecture and be viewed under a microscope. He used this

technique to study neurons and their processes; later, he proposed the “Reticular Theory” on how the central nervous system is composed. This theory stated that the central nervous system was comprised of continuous nerve fibers that allow for diffuse propagation of impulses through the network known as a *syncytium*[65]. His theory would later be challenged by Santiago Ramón y Cajal, who used Golgi’s technique to create illustrate of individuals neuron[66]. In Cajal’s drawings he, most importantly, described the small processes of the neurons called the dendritic spines. This illumination into the components of the neuron allowed his proposed idea of “Neuron Theory” to come into dominance[66]. Neuron theory contrasted with the reticular theory, as it purported that the central nervous system was made up of individual cells, called neurons, that were connected to each other via synapses formed by the dendritic spines[65,66]. These opposing theories led the two men to vehemently dislike each other, but it did not prevent the both of them being jointly awarded a Nobel Prize in 1906 for “Revealing the Inner Beauty of the Nervous System”[67]. The Silver Reaction is now referred to as the Golgi stain, with some variants of the stain being created later on. The original stain is still used today, with some slight modifications[14]. One new variant is the Golgi-Cox stain and it was created in 1891 by W. H. Cox, a German scientist[68]. This variant used mercuric salts to stain the neurons instead of silver nitrate, the original developing agent used in the Silver Reaction. The substitution, along with a few other modifications, allowed for more consistent staining of the dendritic processes.

It was our goal to use Golgi staining to help elucidate what effect aging has on dendritic spine morphology in late age ASD postmortem brain samples. When this technique needed to be optimized for fixed brain tissue, we switched to Golgi-Cox

staining and used it to create a developmental timeline of synapse formation starting at late prenatal development (E18.5) to postnatal day 16 in mice. We chose these stages in mouse development as we believe there are not enough studies that utilize Golgi staining and mouse embryonic brains. This project seeks to create a technique that is successful in visualizing neurons in the developing mouse brain as well as supplementing this investigation with immunofluorescence to discern the connection between adhesion proteins and dendritic spine morphology so that it can applied to future studies for the effects ASD has on them throughout a lifetime.

CHAPTER 2: METHODS AND MATERIALS:

MOUSE BRAIN ACQUISITION:

Embryonic mouse brains were harvested at E18.5 from CD-1 mice from the Charles River. The embryonic mouse brains were acquired after the dam was euthanized (AUP# A211). The sex of the embryos was determined by morphological differences in the external genitalia[46]. Tail snips were taken to confirm sex on selected tissue samples using PCR, using forward primer 5'- CGA ACT CTG GCA CCT TTC A -3' and reverse primer 5'- CAT GGG TCG CTT CAC TCT ATC -3' targeting the *Sry* gene as well as forward primer 5'- GAG TGC CTC ATC TAT ACT TAC AG -3' and reverse primer 5'- TCT AGT TCA TTG TTG ATT AGT TGC -3' for the DXNds3 gene on the X chromosome. Samples dedicated to the IF protocol were immersed in 2-methyl butane over dry ice in a silicone mold for at least 1 minute to ensure samples were thoroughly frozen, this was done after initial tissue fixation in 4% Formaldehyde. Tissue samples were then placed in a -80°C freezer overnight or longer, to ensure the sample was completely frozen before cryo-sectioning. Postnatal mice were acquired from an adjoining lab (AUP# A198b), and tissue was dissected following the protocol outlined by Collins et al. 2018[47]. Brain tissue was sliced in half, down the midline, to separate the two hemispheres to allow for an in parallel study using immunofluorescence and Golgi-Cox staining.

FIXATION:

Brain tissues were immersed in 4% Formaldehyde for 48 hours at 4°C for the IF samples. Golgi-Cox samples were not pre-fixed before staining impregnation

GELATIN-COATED SLIDES:

0.2g of Gelatin type B was mixed in 200ml of heated water and stirred until the gelatin had dissolved. After the gelatin solution cooled to room temperature, 0.02g of Chromium Potassium Sulfate was added and stirred until also dissolved. The solution was then transferred to a wide rimmed container to allow dipping of glass slides, up to seven times, to coat thoroughly. Slides were then placed in a wire rack so the excess could drop off, leaving an even coating of gelatin on the slide to allow for better sample adhesion. Gelatin Solution is stable for up to 6 months.

GOLGI-COX IMPREGNATION:

The Golgi-Cox solution (5% potassium dichromate; 5% potassium chromate; and 5% mercuric chloride) was prepared 24hrs in advance of tissue impregnation to allow precipitate to settle to the bottom of the container, and then removed before impregnation of brain tissue. It was noted that if the potassium dichromate and potassium chromate were combined first, then mixed with mercuric chloride, there was no precipitation. Brain tissue was allowed to incubate in solution in the dark at 4°C for 2 weeks.

Lab safety protocols dictated that a disposable lab cover be worn over cloth lab coat, two layers of nitrile free gloves, and protective eye wear, which must be worn when handling the powdered chemicals, due to the severe hazards associated with them. All work was done in a fume hood to avoid particle inhalation or spread. All items that potentially came in contact with the solution were disposed of, requiring the necessary

materials to be plastic and easily replaceable. If not replaceable, items could be washed thoroughly, but rinse water must be collected to be disposed of by Chemical Safety.

CRYOSECTIONING:

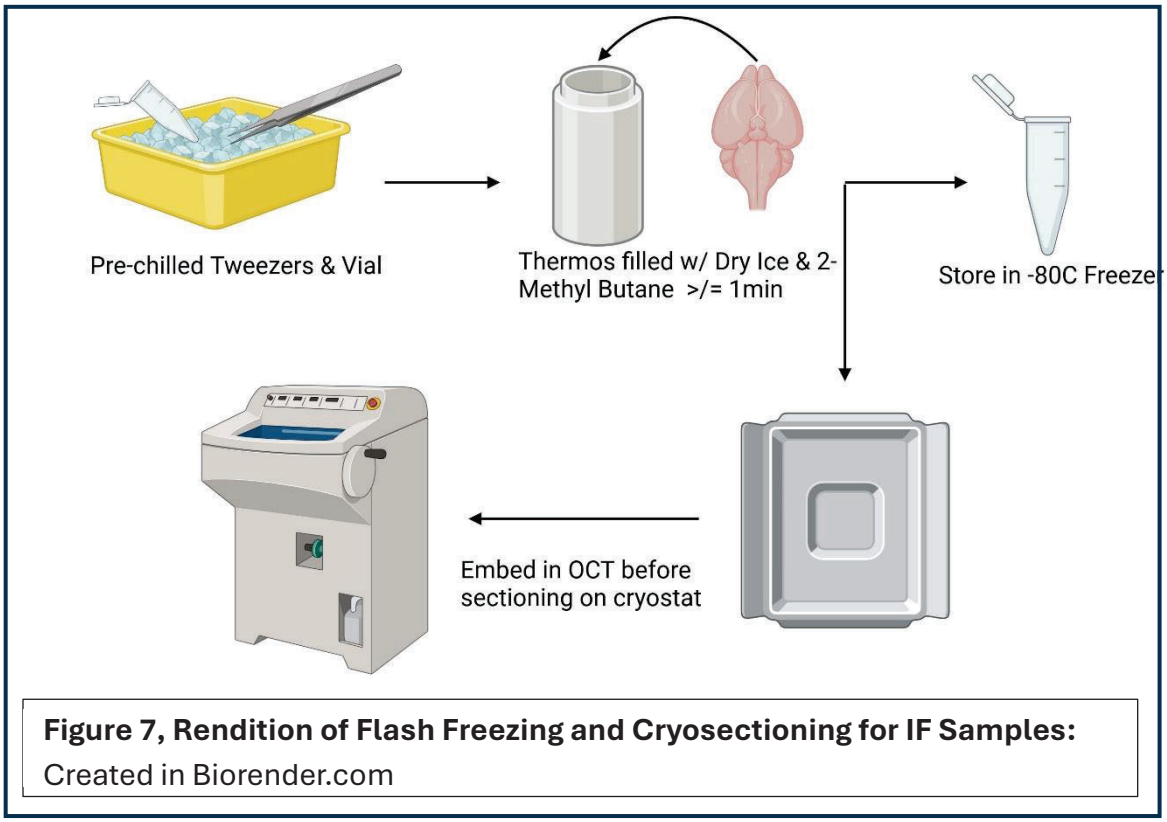

Figure 7, Rendition of Flash Freezing and Cryosectioning for IF Samples: Created in Biorender.com

After impregnation, the Golgi-cox tissue samples were switched to a cryoprotectant solution (20g sucrose, 15ml glycerol, and 85ml deionized water), for 3 days at 4°C. IF tissue samples, after fixation, were immersed in a 30% sucrose solution before being flash frozen using methyl butane and dry ice first then frozen into plastic molds with OCT compound. IF tissue samples then were placed in a -80°C freezer for at minimum 24hrs prior to cryosectioning. OCT compound was prechilled for 30 minutes prior to embedding, tissue block was then frozen again in plastic mold that was in contact, but not submersed, with the methyl butane and dry ice. Golgi-Cox samples

were not flash frozen and instead simply embedded in OCT inside the cryostat at -35°C then moved into the -80°C freezer for a minimum of 24hrs. This was to ensure samples are thoroughly frozen before sectioning at 25µm for IF, and 100µm for Golgi-Cox samples. Figure 7 is a visualization of this process to enhance understanding of flashing freezing and the cryosectioning processes, as well as to show an effective setup for this protocol.

Golgi-Cox and IF samples were both sectioned on a Thermo Fisher Scientific CryoStar NX 50 Cryostat at -35°C. Golgi-Cox sections were adhered to a gelatin-coated slide and sections were kept frozen in a -80°C freezer until needed. Alternatively, if samples were sectioned on a vibratome, the cut sections were placed in a 24-well plate with PBS. Samples in well plates could only be stored for 48hrs at 4°C before tissue integrity started to dwindle. For cryosectioned samples, a small brush is required to delicately press sections to adhere correctly to the slide. IF samples were adhered to superfrost plus slides and kept in the -80°C freezer until needed for IF procedure. Slides with less inherent adhesion properties were not effective in retaining samples on slides during IF staining protocols.

Adjusting cryostat temperature degree by degree is necessary for achieving the proper conditions for successful section of tissue. Briefly swiping a gloved finger over the IF samples was useful for maintaining the integrity of slice when the sample was temporarily too cold but too sensitive to thaw if the temperature was raised. When the sample was too warm, briefly setting a cold metal block helped to bring the sample to the desired temperature before resuming the sectioning process. Samples could become too warm due to outside air exposure, or from exhaled air while sectioning. It

can be difficult to maintain the proper conditions during cryosectioning, so it is imperative to be prepared for obstacles.

DEVELOPMENT OF GOLGI-COX STAIN:

For cryosectioned samples, a dropwise method was implemented for development. Slides were washed in deionized water twice, for 5 minutes. One droplet of diluted 10% ammonia was added to each tissue sample and left to sit for 15 minutes before two 5 minute water washes were done. After this, sodium thiosulfate was added and checked every 2 minutes to prevent over development, this would lead to the tissue integrity being compromised. A final water wash was performed before the slide was dried carefully with a paper towel. Due to excess water being directly on sections, Fluorgel Mounting Medium was used to attach coverslips instead of Permount. These slides were then stored in a dark container at room temperature overnight to cure the gel. Once the gel was cured, slides were moved into 4°C refrigerator to prevent degradation of samples if left at room temperature.

Golgi-Cox slices that were collected in PBS filled wells were developed in 20% ammonia for 10 minutes, washed twice in deionized water for 5 minutes each, and then in 1% sodium thiosulfate (Thermo Fisher) for 10 minutes. A full-face respirator mask was used to prevent facial exposure to ammonia. Slices were washed in deionized water for 5 minutes twice. Samples were mounted onto gelatin coated slides. Sections were then allowed to briefly dry before using Permount Mounting Medium to attach a glass coverslip to slides. This procedure is best suited for samples sectioned on a vibratome.

IMMUNOFLUOROESCENCE:

IF tissue samples were sliced to 25μm on a cryostat. To ameliorate autofluorescence, samples were photobleached with a white LED light source for 4hrs. Sections were imaged before and after photobleaching to ensure adequate bleaching. They were also covered in PBS during photobleaching to prevent the tissue from drying out. Two 10-minute washes in PBS were then conducted before incubating slices in 5% Goat Serum for 2 hours at room temperature. The primary antibodies used were: Synapsin1 (Synaptic Systems, 1:1000), N-Cadherin (Cell Signaling Technology, 1:200), and PSD-95 (Synaptic Systems, 1:500). These antibodies were diluted in 2% Goat Serum according to manufacture guidelines for IF protocols. Due to the low dilution ratio of N-Cadherin, the sections were encircled with an ImmEdge Pen to create waterproof edges around tissue samples to prevent antibody solution from spreading indiscriminately across slides. Slices were incubated in the primary antibody solution for 48 hours at 4°C, in a dark and humid container. M.O.M Blocking Reagent (Vectorlabs) was used according to the printed instructions and incubated for 1hr at room temperature between primary and secondary incubations[69]. Afterwards, slices were washed once for 2 minutes in PBS. Secondary antibodies were added (Alexa488 (Mouse), Alexa647 (Rabbit), and Alexa568 (Guinea Pig)) to a 2% Goat Serum, and incubated with the slices for 2 hours at room temperature in a dark environment. Another wash was performed along with removal of the wax circles before applying the Fluoromount Gel with DAPI to each sample then attaching the coverslip.

IMAGING

IF samples were initially imaged on an EVOS microscope to ascertain whether the IF protocol had been successful. When confirmed, samples were moved to an Olympus FV1000 confocal microscope for further imaging. Images were taken at 10x and 60x magnification at 8.0us/pixel with 20 slices. All 60x magnification photos were taken within the area imaged at 10x magnification. Golgi-Cox samples were imaged on a Ziess Imager.M2, using Neurolucida's imaging software. This program allows for 3D models and accurate counting of dendritic spines on selected neurons, along with identification of morphology.

ANALYSIS: Neurolucida

The Neurolucida was used to record the morphology of the dendritic spines and calculate an average count of each morphology. This analysis was important for determining the predominant morphologies associated with varying developmental time points as well as acquiring the total number of dendritic spines.

ANALYSIS: Fiji/ImageJ

Images that were captured at 60x magnification from the confocal microscope were used to analyze N-Cadherin in mouse brain tissue samples. The image was split into three channels, based on the wavelength used in the microscope. Each channel was z-projected to max intensity before a threshold was assigned to each by Fiji. The threshold was then adjusted by an increase of 20 units across all samples. Once all the channels had been adjusted for threshold, the synapsin1 and PSD-95 channels were colocalized together using the colocalization plugin available in Fiji. This colocalization

detected all points in the two channels where there was overlap between synapsin1 and PSD-95. The overlap indicated a positive synapse result as the antibodies are pre- and post-synaptic markers. The colocalized image then adjusted to exclude all points measured over 10μm^2 to exclude any over fluorescing areas. The mask that was created from this operation was then colocalized with the N-Cadherin channel. This colocalization allowed for the identification of N-Cadherin positive synapses. Another mask was created to fit with the parameters outlined previously on size. Once the two masks were created, the images were then subtracted from each other to acquire information on N-Cadherin negative synapses. A mask of the N-Cadherin negative synapses was created as well from this operation to for easier visualization. A particle analysis was implemented upon each mask created to obtain information on the synapse size, the number of synapses detected, and the area occupied by synapses within the imaged area. The acquisition of the area occupied by synapses was later used to confirm the accuracy of the subtraction of N-Cadherin positive synapse mask to the All Synapse mask as when the area of the N-Cadherin synapse occupation was added to the N-Cadherin negative area they summed to the total area measured from the All Synapse mask. To normalize the data measurements acquired during the particle analysis, the tissue area within the imaged channel needed to be determined. This was done by thresholding the image of the tissue until only the stained tissue was highlighted, this was necessary as some tissue samples had small tears that were visible under the confocal microscope. The area that was highlighted was then measured so that an area value could be saved and utilized to normalize data points

during analysis. Once all measurements were taken, the data points underwent statistical analysis in SigmaPlot.

Analysis: SigmaPlot

Data points gathered from Fiji in ImageJ underwent statistical analysis in SigmaPlot 13. A variety of data points were collected from particle analysis in Fiji. Measurements for the total number of synapses, number of N-Cadherin positive synapses, number of N-Cadherin negative synapses, total area occupied by synapses, area occupied by N-Cadherin positive synapses, and the area occupied by N-Cadherin negative synapses were normalized to the tissue area was calculated through thresholding the tissue as previously described. In this experiment mouse brain tissue was collected from embryonic day 18.5, postnatal day 6, and postnatal day 16. There were two biological replicas from the embryonic day 18.5 mice brain samples, three biological replicates for postnatal day 6, and three biological replicates for post-natal 16. Each biological replicate had varying technical replicates but in total had 12 technical replicates for each age group, for example at postnatal day 6 there were three male mouse brains that had four images taken from each brain to be analyzed. This data was then averaged together to create an average for each biological replicate. The standard deviation was then calculated from the data set. Due to unforeseen difficulties in optimizing the freezing and section of the embryonic tissue there was insufficient data gathered for proper statistical analysis. If enough biological replicates had been used, as there were only two embryonic day 18.5 replicates, then the averaged data would be inputted into One-Way ANOVA's to detect statistically significant differences between the age groups across selected dependent variables. Dependent variables then

analyzed would include N-Cadherin positive synapse size, N-Cadherin negative synapse size, density of N-Cadherin positive synapses, density of N-Cadherin negative synapses, the total number of synapses over time, total number of N-Cadherin positive synapses over time, and total number of N-Cadherin negative synapses over time. Two-Way ANOVAs would then be implanted last to discern differences between the age groups as well as the N-Cadherin positive and negative synapses. Post-hoc analysis tests would be chosen by SigmaPlot to best fit the data. With the low sample size, bar graphs were used to display averaged biological replicate data across each time point with the individual data points displayed and standard deviation associated with each mean. T-tests were also then implemented to discern statistical differences between postnatal day 6 and postnatal day 16 as their sample size was consistent and large enough to analyze. Plotted data was then looked at to discern trends within the data.

Chapter 3: Results

Optimization of Golgi Staining

Our process started with the intent to use a Golgi-Kopsch staining protocol derived from Hustler and Zhang 2009 to stain adult human neurons to investigate the dendritic spines[14]. This technique utilized a Potassium Dichromate, Distilled Water, Sucrose, and Formaldehyde solution. A 3mm thick tissue block was immersed in the solution for 2 weeks at 4°C in the dark. After two weeks of incubation the solution was removed and replaced with a 0.75% Silver Nitrate developing solution. The human tissue was immersed in the developing solution for 3 days at 4°C. At the end of this period the tissue developed small black crystals on the surface, these needed to be brushed away before sectioning on the vibratome. The prepared tissue was then sectioned at 120µm on a vibratome. Tissue slices were mounted onto gelatin coated slides, dehydrated and cleared, then coverslipped with Permount Mounting Medium.

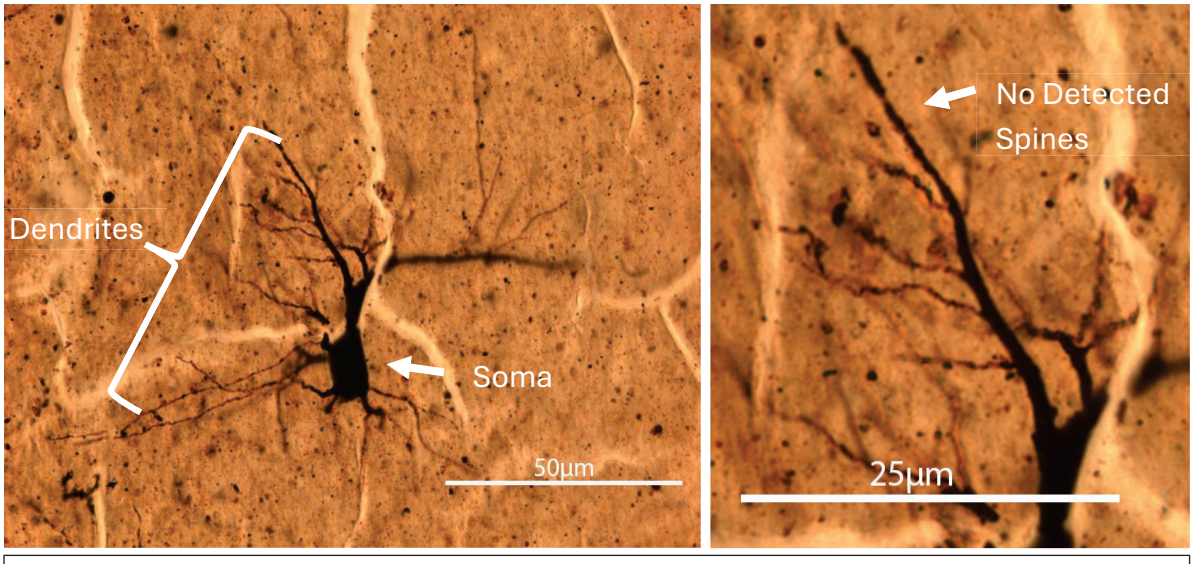

Figure 8, Original Golgi-Kopsh Stain Technique: Performed on human brain tissue from Broadmann's Area 21. Neuron anatomy labeled identifying the soma, dendrites, & axon. Right images highlights the lack of dendritic spine staining.

We used control human brain tissue obtained from Harvard Brain Tissue Resource Center. Control tissue was used first so that we could optimize the staining process before being granted access to ASD brain tissue samples for further experimentation. The tissue was obtained from Broadmann's Area 21, also known as the posterior middle temporal gyrus. The results of the original technique had adequate staining of the neuronal body, axon, and dendrites but as highlight in the Figure 8, there was no visualization of the dendritic spines. Due to the limited amount of human brain tissue, we decided that further optimization would be done on mouse brain tissue instead. A postulation of why staining was not adequate was that the development with Silver Nitrate was too short, preventing the spines from being stained properly. Development time was extended up to 7 days but there no was visual improvement of spine staining. Another potential reason for the lack of dendritic spine staining was that the postmortem index on the brain tissue samples was 52.28 hours, longer than the recommended time for brain tissue acquisition so the dendritic spine processes may have been damaged or lost over time. The undetermined amount of time in formalin may have also prevented the impregnation step of the Golgi-Kopsch technique from achieving full effectiveness or affected the ability of the Silver Nitrate to work during development of the stain.

The next step was to try another variant of Golgi staining, and if successful couple this technique with immunofluorescence. The Golgi-Cox technique used Potassium Dichromate, Potassium Chromate, and Mercuric Chloride for the impregnation step and 20% Ammonia and 1% Silver Nitrate for the development. Using P20 brains for optimization, they were prefixed for 48 hours in 4% Formaldehyde.

Tissue then transferred to the Golgi-Cox impregnation solution for two weeks at 4°C in the dark. The tissue was then sliced on the vibratome at 100µm in a 30% sucrose solution. 120µm sections used too much Permount mounting medium and had difficulty curing so section thickness was reduced to 100µm. Sections were placed in a 24 well plate, as later they would be uses for IF staining. Sections were first washed in PBS for five minutes before being immersed in 20% ammonia. They were immersed in the ammonia for 10 minutes before being washed again for 5 minutes, twice. 1% Sodium Thiosulfate was then used for 10 minutes and washed again afterwards. During the Sodium Thiosulfate part, sections became clear. All of the development process was performed on shaker to gently rock the samples. Removing the need to clear with xylene. Sections were then mounted onto gelatin coated slides. Fluorogel was then used to adhere the coverslips to the slides.

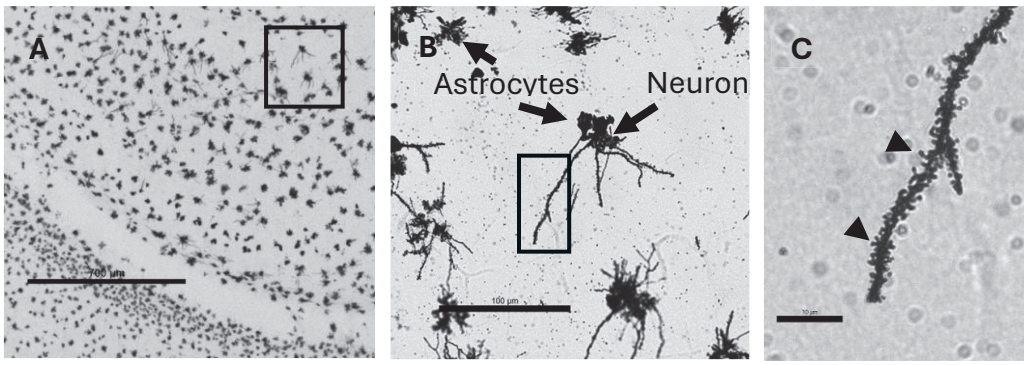

Figure 9, Golgi-Cox Technique in Mice: First Golgi-Cox stain that was prefixed in 4% Formaldehyde. Tissue sectioning on a vibratome. Image A is a 10x image from the hippocampus, with a 700µm scale bar. Image B is at 20x magnification, focusing on the highlighted region in A. Glia can be seen obscuring soma and dendrites. Image C is at 100x magnification, from highlighted region in B. Arrows heads are indicating dendritic spines.

Once the slides were cured, they were imaged on a Ziess Imager M.2. As highlighted in Figure 9, staining of the dendritic spines was successful. Interestingly, we noticed that there was obstruction of the soma as well as the dendrites from glia cells, specifically astrocytes. When looking back into the literature, it was discovered that prefixing tissue in aldehydes caused preferential staining of glia[70,71]. The prefixing with 4% Formaldehyde was then removed from the protocol. With the Golgi-Cox technique proven to be successful we moved from sectioning on the vibratome to the cryostat. This was because our initial goal was to combine IF with the Golgi-Cox, and cryosectioning is commonly used for IF. The cryostat also would give support to the brain tissue, from being embedded in OCT, making coronal sectioning easier whereas on a vibratome there would be complications. The cryostat also allowed more control when doing thinner sections.

After following the same impregnation protocol the tissue was immersed in a 30% sucrose solution for at least 3 days. The tissue was then sectioned at varying temperatures, but there was either shattering of the tissue or the tissue had thawed and wasn't sectioning properly. Looking back at different protocols a new cryoprotectant solution was used where now it was 15% Glycerol and 20% Sucrose[72]. This change fixed the shattering issue in the cryostat, which tissue now being consistently sectioned at -35°C. Switching to a dual temperature cryostat also facilitated sectioning as it kept the tissue block at a more consistent temperature. Once sectioned, the tissue was adhered to gelatin coated slides and pressed delicately in place with a brush before then kept in a -80°C freezer until ready for development.

For development, we used a transfer pipette to add the developing chemicals in a dropwise fashion. Immersing the slides in liquids increased the chance of the tissue sliding off. Differing from the vibratome sections, the cryostat sections developed faster but were susceptible to tissue integrity loss. We postulated that the cryostat increased the porosity of the tissue, or potentially the glycerol made the tissue vulnerable. To deal with these new issues, the ammonia time was decreased to 5 minutes as well as the sodium thiosulfate. This change limited the staining of the neurons. Another change was made to dilute the ammonia to 10% and the Sodium Thiosulfate to 0.5%. The ammonia time was increased to 8 minutes and the Sodium Thiosulfate was monitored every two minutes to preserve tissue integrity. The slides then had the excess water removed by gently wiping it down with a paper towel and immediately coverslipped with Fluoromount Gel used as the mounting medium. The slides were allowed to cure overnight at room temperature before being moved into the 4°C refrigerator. These changes proved to be successful in the P16 brain tissue, there was successful staining of the whole neuron with no glia obstruction.

Optimization of Immunofluorescence

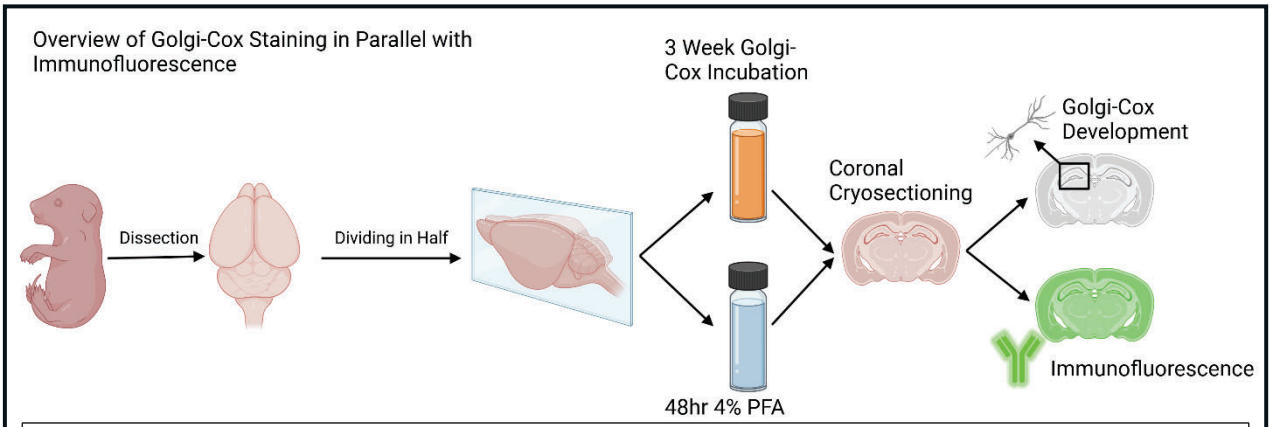

Figure 10, Overview of Golgi-Cox & IF in Parallel Protocols: A diagram visualizing the protocol for dissecting brain, incubation periods, cryosectioning, then final development or antibody staining. Created in Biorender.com.

Our original intent with immunofluorescence (IF) was to combine it with Golgi-Cox staining so we could investigate if certain adhesion proteins are associated with a specific dendritic spine morphology. We started this process with the original Golgi-Cox technique on a P20 mouse brain. We followed the protocol where after development of the Golgi-Cox stain the samples were permeabilized and blocked in a 0.5% TritonX-100 and 5% Goat Serum solution, overnight at 4°C. After washing in PBS, primary antibodies (PSD-95, 1:500, Santa Cruz; SynCAM1, 1:100, Synaptic Systems; Synapsin, 1:1000, Synaptic Systems) were diluted in 5% Goat Serum. The tissue was incubated in the primary antibodies in a 24 well plate at 4°C for 48 hours. Another wash was performed and then tissue was incubated for 2 hours at room temperature with the secondary antibodies diluted in 2% Goat Serum. After another PBS wash, the tissue sections were mounted onto glass slides and cover slipped.

When these samples were imaged, non-specific binding combined with autofluorescence was observed, as highlighted in Figure 11. The results of this experiment necessitated a different direction where instead of the two techniques being combined, they would now be performed in parallel. To do this we split all future mouse tissue samples down the midline where one half would follow the Golgi-Cox route and the other would undergo IF staining (Fig. 10).

The IF tissue samples were prefixed in 4% formaldehyde for 48 hours at 4°C. They were then immersed in the same glycerol cryoprotectant solution as the Golgi-Cox samples for at least 3 days and kept in the 4°C refrigerator until cryosectioned. The tissue samples were removed from the cryoprotectant solution to be embedded in OCT compound and frozen inside the cryostat at -20°C. Samples were then sectioned initially

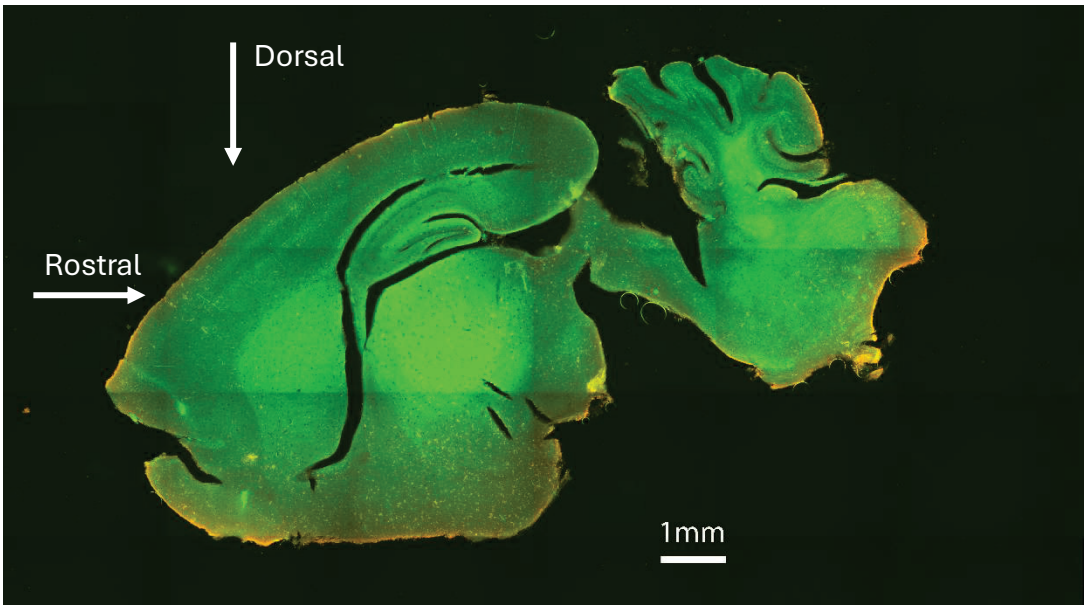

Figure 11, Combination of Golgi-Cox and IF in Mouse Brain: A sagittal section of a male PND20 mouse brain. Tissue underwent Golgi-Cox staining and IF. Stained for Synapsin (not shown), PSD-95 (Green), SynCAM1 (Red). No indication of specific binding. Magnification set at 40x.

at -16°C. Interestingly, the tissue did not appear to be fully frozen and when sectioned the tissue section would be unviable. Varying temperatures were tried as well as moving samples to a dual temperature cryostat, as it ensured better temperature consistency. These changes provided no progress in ensuring the samples were thoroughly frozen. Freezing the samples embedded in OCT with 2-methyl butane and dry ice did also not properly freeze the tissue. Our postulation about the inability to freeze the embedded tissue was that the glycerol had over impregnated the tissue, causing the freezing point of it to drastically lower. Added with the OCT acting as an insulator and not allowing the full cold of the dry ice and methyl butane to fully penetrate the tissue, we decided to flash freeze the tissue directly in 2-methyl butane and dry ice with no OCT. These samples were then placed in a -80°C overnight to ensure tissue was properly frozen. At time for sectioning, the tissue was embedded in prechilled OCT then flash frozen again to solidify the OCT. When these samples were then cryosectioned, the tissue was thoroughly frozen and usable for IF. This process of optimizing the freezing and cryosectioning process of the embryonic brains led to a low sample size in the end for the experiment. This was a limited resource in the lab and it took many attempts and months to perfect the freezing process and then successfully cryosection the tissue for IF leading to there not to be sufficient enough data for analysis later on in the experiment.

We sectioned all IF samples at 25μm as previous sectioning at 10um resulted in tearing of the tissue. After following the immunofluorescence staining procedure outlines in the methods section, samples were imaged on an EVOS microscope. Initial images showed autofluorescence, which was not specific to our antibodies (i.e. tissue without

antibody incubation still exhibited fluorescence). To ameliorate the autofluorescence, tissue was photobleached with a white LED light for 4hrs (Fig. 12). This was successful, and every sample used was imaged before and after photobleaching to ensure all received adequate bleaching before moving forward with the IF staining.

Due to our lab specializing in mainly human cell culture models, most of the antibodies used are derived from mice. To counteract this, our IF protocol added a second blocking process between the primary and secondary incubations utilizing the Vector Labs Mouse on Mouse (M.O.M) blocking reagent to make sure that the secondary mouse antibodies would only attach to their specific epitopes and not non-specifically.

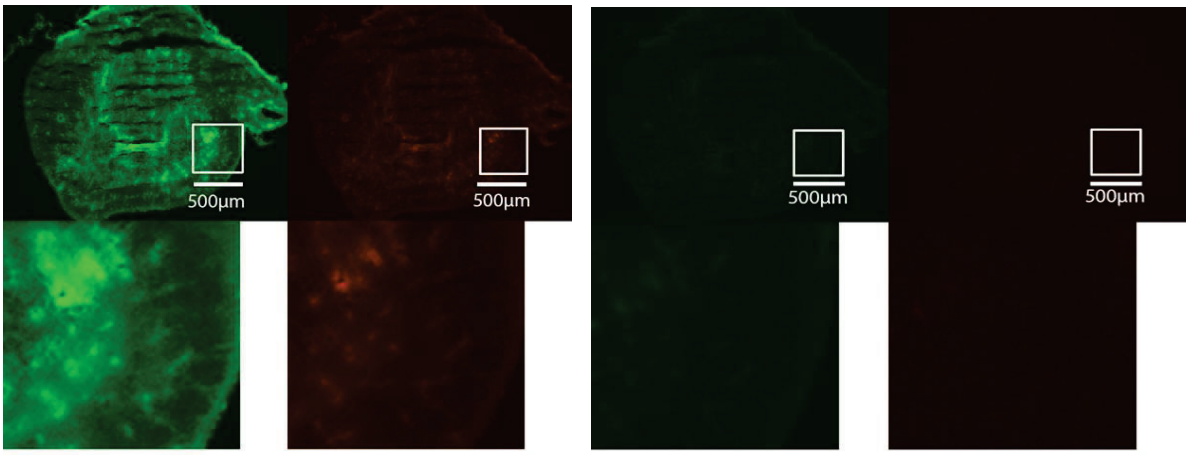

Figure 12, Pre- & Post-Photobleaching in Mice Brain Sections: A is a pre photo bleach of an E18.5 male mouse brain section. Imaged at 40x magnification. Area enlarged to enhance visualization of auto-fluorescence. Image B is the post photo bleach of same sample of the same sample after 4hrs of white LED light.

GOLGI-COX STAINING:

Before delving into the finalized results for the optimized Golgi-Cox staining procedure a brief review of the optimized protocol will be outlined. Brain tissue undergoing the Golgi-Cox method were initially impregnated with Potassium Dichromate, Potassium Chromate, and Mercuric Chloride. This chemical solution was able to fix the tissue and prevent degradation. Removing pre-fixing with 4% Formaldehyde also prevented preferential glia staining. Afterwards the samples were embedded in OCT media and left to fully freeze in an -80°C freezer for at least 24 hours. Once tissue was fully frozen it was moved into the cryostat where it would be

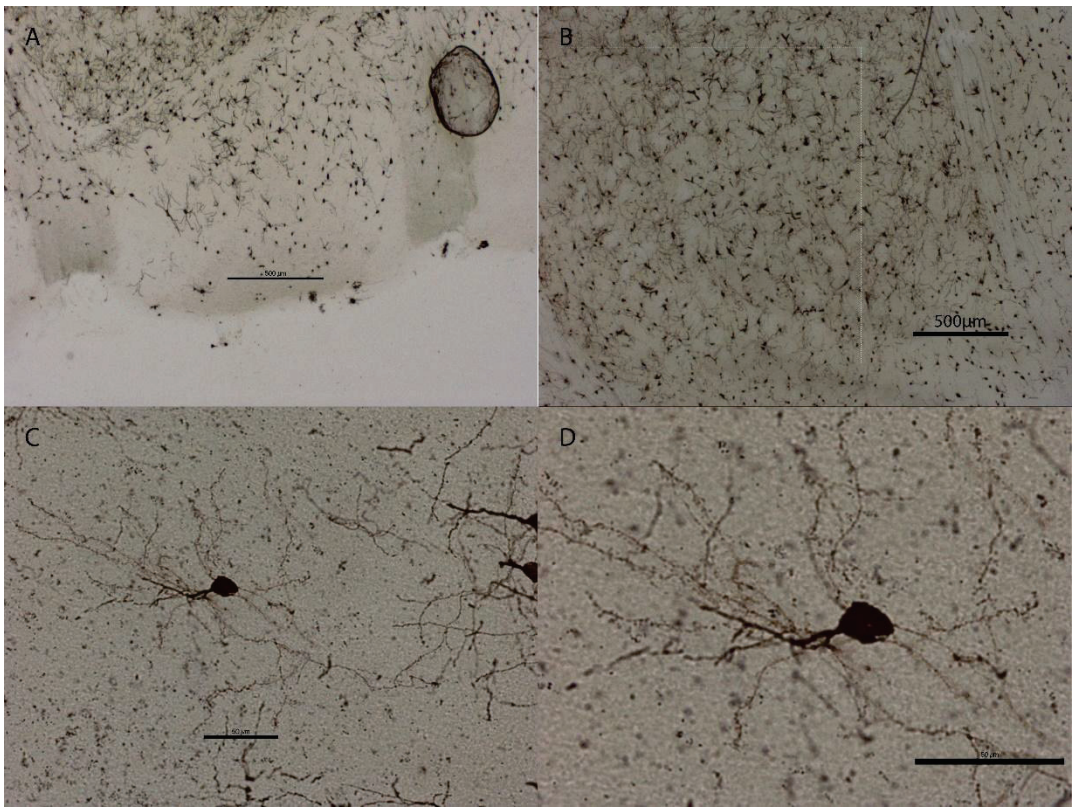

Figure 13, Optimized Golgi-Cox Staining: Cortical pyramidal present in the sensory cortex of a PND16 male mouse brain. Image magnification starts in A at 25x, B at 100x, C at 200x, and D at 400x. Neurons are now preferentially stained instead of glia, compared to Figure 9.

sectioned to a thickness of 100µm. For development the slides underwent the altered development protocol that was changed to help prevent over development. Once the sections were coverslipped and allowed to set, they were imaged on an Ziess Imager M.2 that was connected to the Neurolucida software, which has the function of neural tracing. Figures 13 & 14 were all taken on the Ziess Imager M.2. The Neurolucida has an Explorer add on which is capable of analyzing the 3D neural tracings measure the number of dendritic spines on each neuron, the number of branches, the amount of different morphologies, and many more functions. Figure 13 & 14 are demonstrative of neurons that can accurately have a tracing overlayed to analyze dendritic spine number and morphology. It can be noted that there was no loss in tissue integrity in Figure 13 & 14, highlighting that there is no need to prefix tissue for Golgi-Cox staining.

This technique combined with the Neurolucida software allowed us to create a foundational basis for to measure the development of synapses across different times points accurately, along with recording what dendritic spine morphology is predominant at each time point.

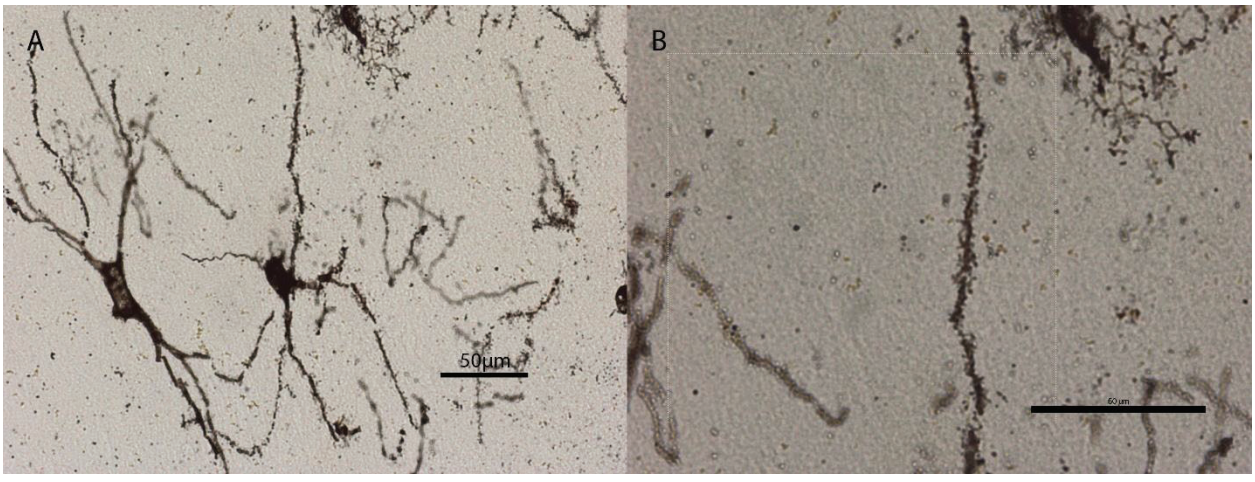

Figure 14, Pair of Cortical Pyramidal Neurons: Derived from PND16 male mouse brain Excellent depiction of dendritic spines. Image A is at 200x and image B is at 400x

IMMUNOFLUORESCENCE:

All samples after cryosectioning were imaged before and after photobleaching for 4hrs to ensure that each sample no longer auto-fluoresced. Once slides were

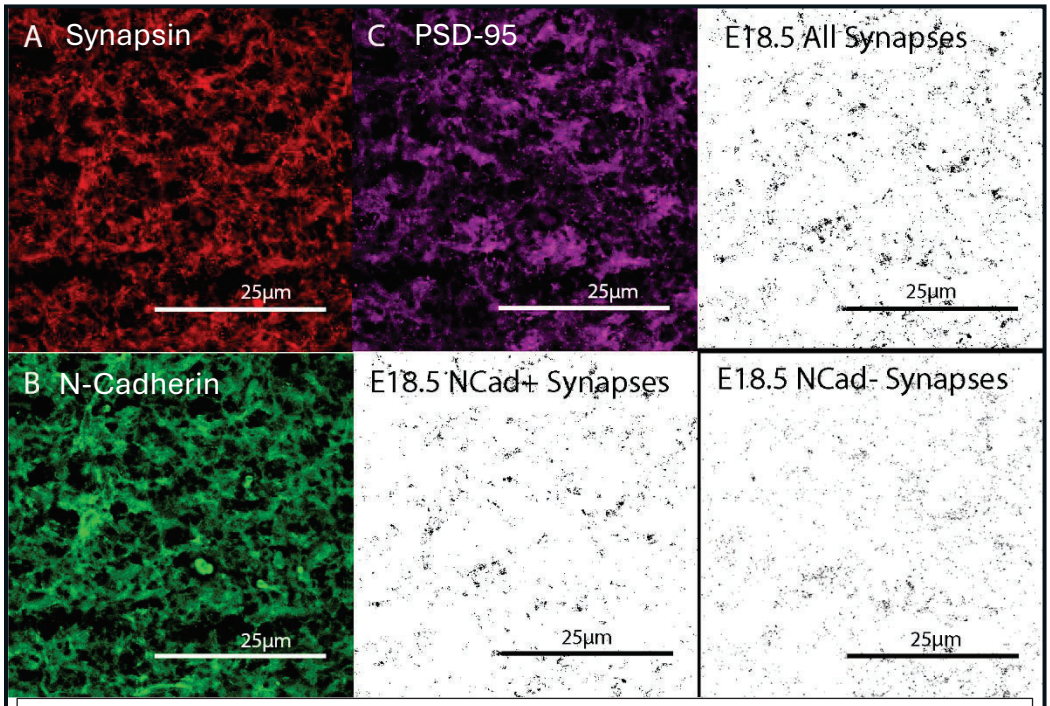

Figure 15, IF Channels & Masks for E18.5: A male E18.5 brain tissue sample captured at 600x magnification. Synapsin is red (A), PSD-95 purple (B), and N-Cadherin (C). Depicted are the Fiji generated masks of both all detected synapses and N-Cadherin positive synapses.

photobleached, the samples were blocked for 2 hours at room temperature in 5% Goat Serum to block to reduce non-specific binding of the antibodies. One PBS wash was performed for 5 minutes before adding the primary antibodies to 2% Goat Serum and incubating at 4°C for 48 hours. Afterwards, another 5 minutes PBS wash was performed. Due to one of the antibodies being derived from mice we utilized the Vector Labs Mouse on Mouse blocking reagent according to manufacturer instructions secondaries in sample. Fluorogel with DAPI was used to stain the nuclear DNA after

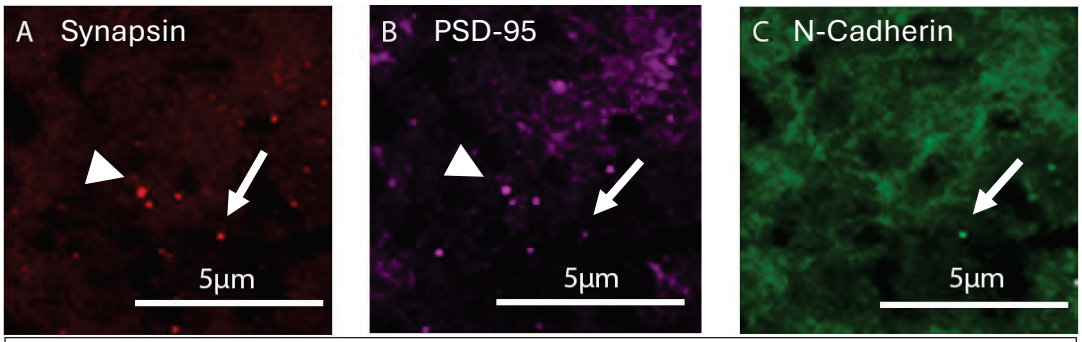

Figure 16, Enlargement of Synapse: Enlarged area from Figure 15. Arrows are pointing towards a N-Cadherin positive synapse and arrow heads to a N-Cadherin negative synapse. Method prevents false positive detections.

Samples were then imaged in the Olympus FV1000 confocal microscope. 20 slices at 8 pixels per second were imaged then later analyzed by Fiji in ImageJ at magnifications 10x and 60x. Data points were gathered from three different age groups: E18.5, PND6,

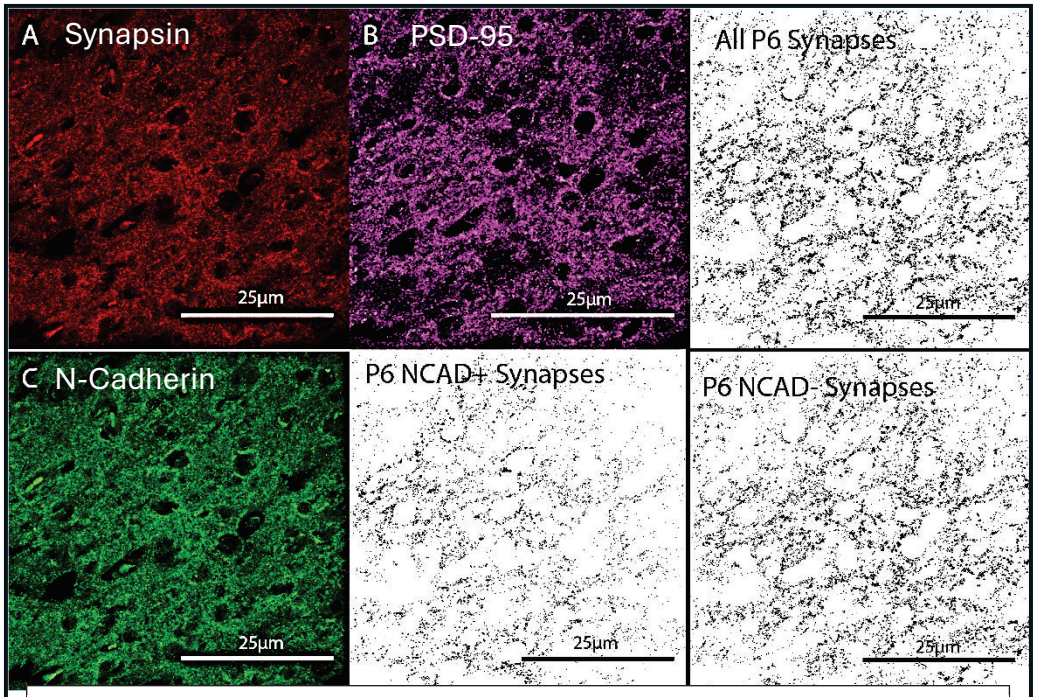

Figure 17, IF Channels & Mask of PND6: A male PND6 brain tissue sample captured at 600x magnification. Synapsin is red (A), PSD-95 purple (B), and N-Cadherin (C). Depicted are the Fiji generated masks of both all detected synapses and N-Cadherin positive synapses.

and PND16 (Fig. 16, 18, 19). Images at magnification 10x were not used for data analysis but all 60x images were. All analysis procedures were performed identically on each group to ensure consistent results. When all samples were imaged, they were analyzed by Fiji in ImageJ to colocalize synapsin1 and PSD-95 to create a colocalized image to indicate which pixel points were synapses. Synapsin1 is a presynaptic marker and PSD-95 is a postsynaptic marker, when overlayed it can be assumed there is a synapse (Fig. 17). Once the synapses were identified the new points were colocalized to the N-Cadherin image channel (Fig. 17). This method reduced the number of false positive identifications by Fiji, increasing the validity of the results. These newly identified n-cadherin synapse masks were then subtracted from the identified over all

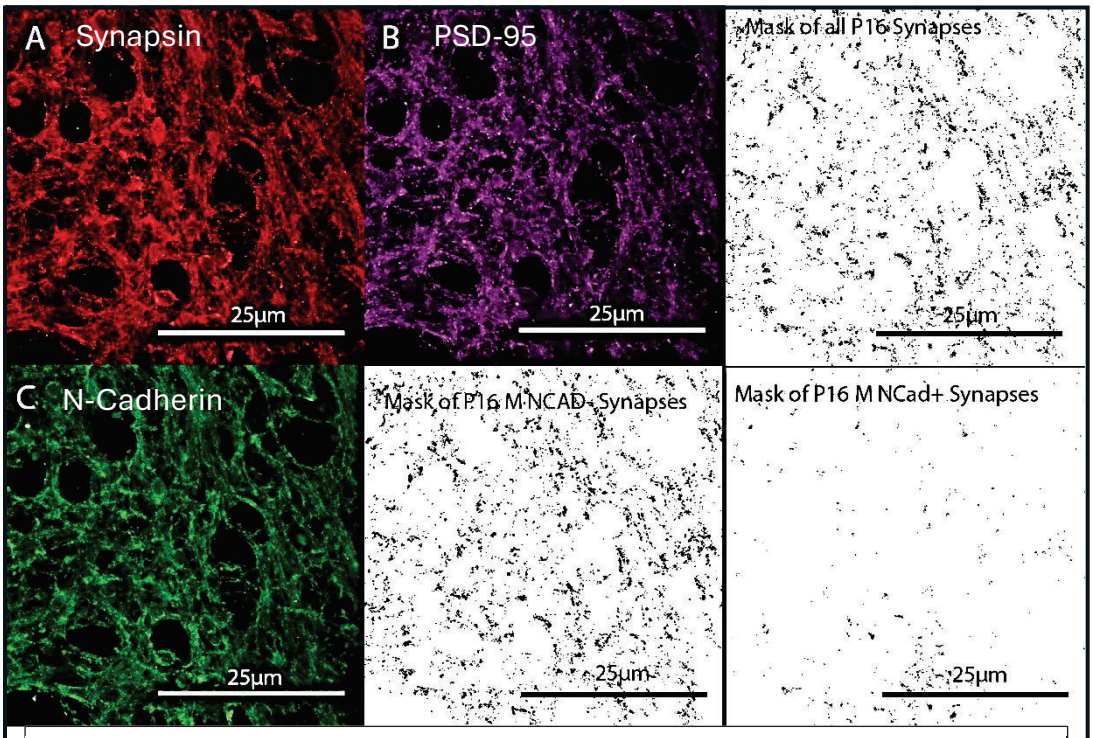

Figure 18, IF Channels & Mask of PND16: Male PND16 brain tissue sample captured at 600x magnification. Synapsin is red (A), PSD-95 purple (B), and N-Cadherin (C). Depicted are the Fiji generated masks of both all detected synapses and N-Cadherin positive synapses.

synapse mask to acquire data on N-Cadherin negative synapses. Data gathered from these operations were then plotted in SigmaPlot.

Analysis of All Identified Synapses

The first bar graph illustrates the total synapse density across time highlighted that at postnatal day 6 there was increased synapse density compared to embryonic day 18.5 and a subtle difference between postnatal day 6 and postnatal day 16 (Fig. 19). Low variation in density can be seen when examining individual data points at embryonic day 18.5 and postnatal day 16, with the largest variation seen at postnatal day 6 (Fig. 19). One-Way ANOVAs were not utilized in this analysis due to the

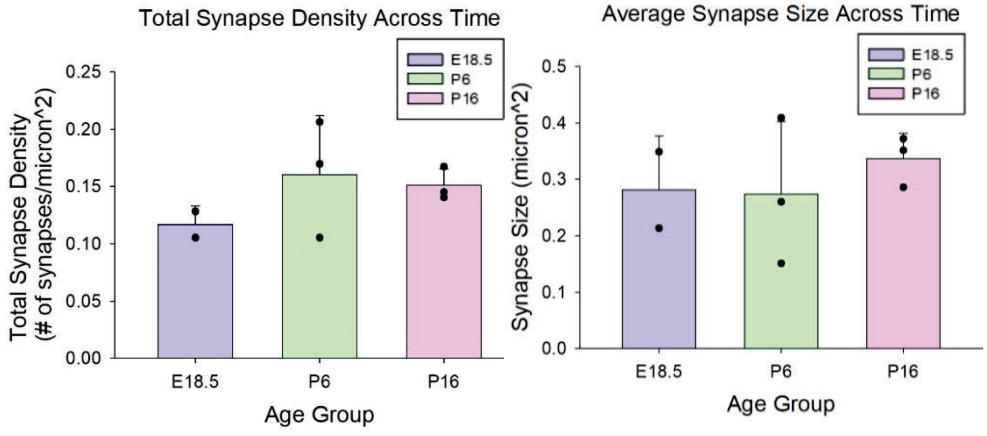

Figure 19, Total Synapse Density and Synapse Size Across Time: Bar graph with averaged means from biological replicates, points are the individual means plotted within the bars. Trends observed in data suggest that largest variation in density occurred at P6 and largest synapse size occurred at P16. Two biological replicates for E18.5, three for P6, and three for P16 with standard deviation included.

insufficient sample size of the embryonic day 18.5 group. A bar graph was instead utilized to help visualize trends within data.

When examining the average synapse size, including both N-Cadherin positive and negative synapses, there were slight observable increases in synapse size at postnatal day 16, which also had low variation between biological replicate averages as seen as individual plot points in bar graph (Fig. 19). There was no observable difference in synapse size between embryonic day 18.5 and postnatal day 6, though there was large variation between the three biological replicates at postnatal day 6 (Fig. 19).

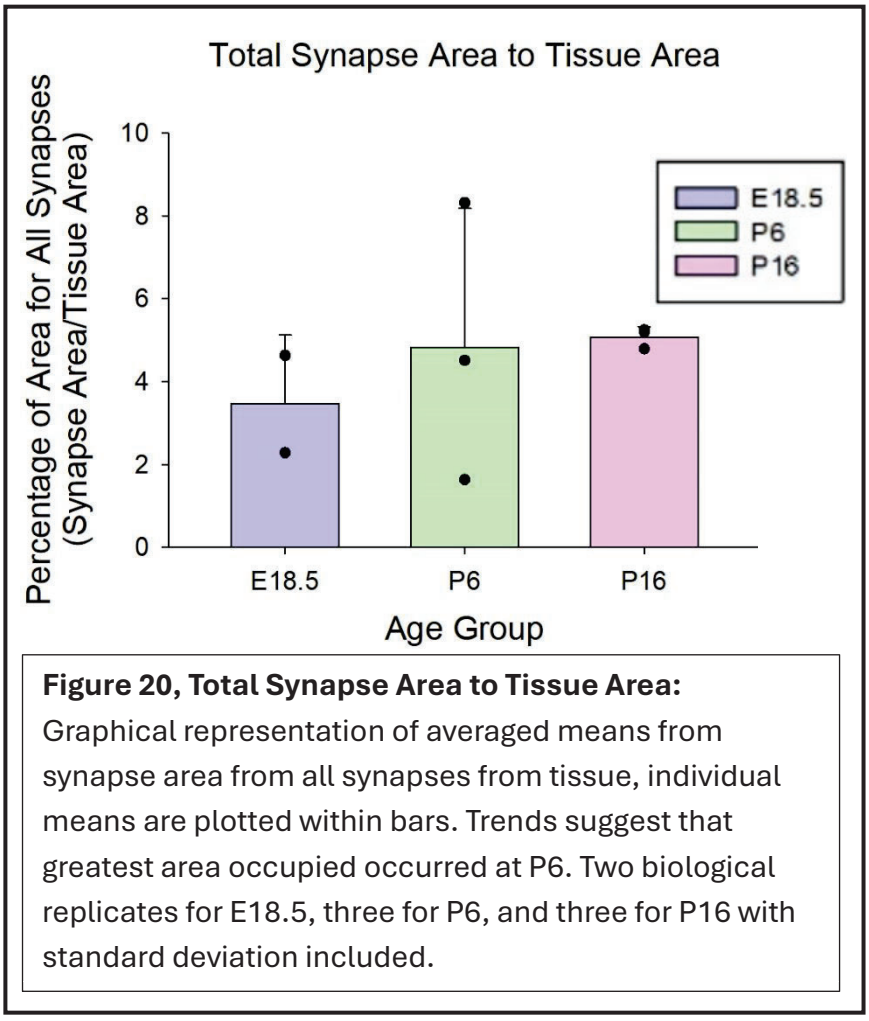

Figure 20, Total Synapse Area to Tissue Area: Graphical representation of averaged means from synapse area from all synapses from tissue, individual means are plotted within bars. Trends suggest that greatest area occupied occurred at P6. Two biological replicates for E18.5, three for P6, and three for P16 with standard deviation included.

The next bar graph illustrates the area occupied by all identified synapses within the measured tissue area mirroring the trends seen in total synapse density and synapse size (Fig. 20). Considerable variation in synapse area was observed at both embryonic day 18.5 and postnatal day 6, the least variation in individual biological replicate plot points was at postnatal day 16 (Fig. 20). T-Test between postnatal day 6 and postnatal day 16 did not reveal any significant differences between synapse density, average synapse size, or the percentage of area occupied by synapses (P-values: 0.387, 0.235, & 0.700).

Analysis of All N-Cadherin Positive Synapses

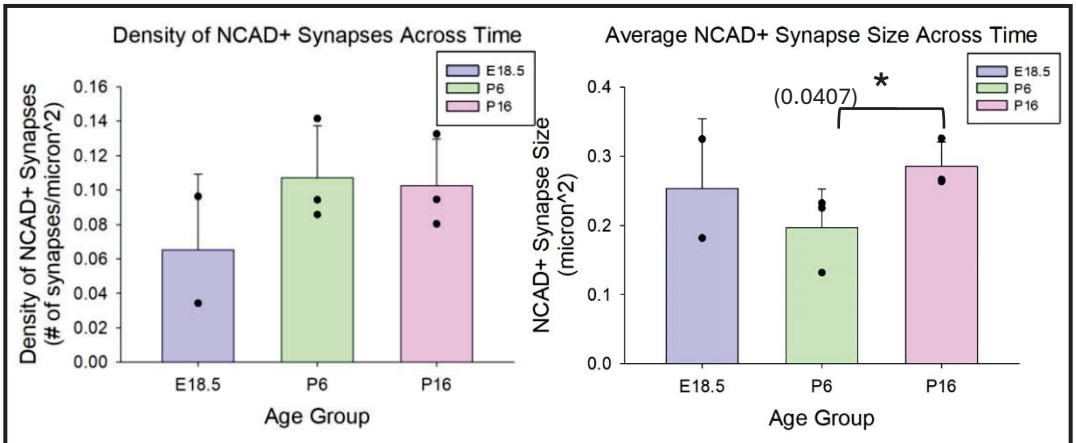

Figure 21, Density & Size of NCAD+ Synapses Across Time: Bar graph illustrating averaged N-Cadherin positive synapse density across time in biological replicates, and right graph the average N-Cadherin positive synapse size. Greatest variation of synapse density seen at P6 and trends in synapse size data suggests largest synapse size to occur at P16. T-Test between P6 and P16 showed significant difference (P-value: 0.0407). Two biological replicates for E18.5, three for P6, and three for P16 with standard deviation included.

Bar graphs created in SigmaPlot using the average of each biological replicate, and overall standard deviation for each time point, were used to identify trends within

the normalized N-Cadherin negative synapse data. Trends observed in the data indicate that at embryonic day 18.5 there was the lowest density in N-Cadherin synapse observed (Fig. 21). There was no discernable difference between postnatal day 6 and postnatal day 16 (Fig. 21). All individual data within each time point had considerable variation between the biological replicates (Fig. 21).

When observing the average N-Cadherin positive synapse size across time, the lowest size was seen at postnatal day 6 (Fig. 21). Slight variation of individual data points could be noticed at each time point for the average N-Cadherin synapse size

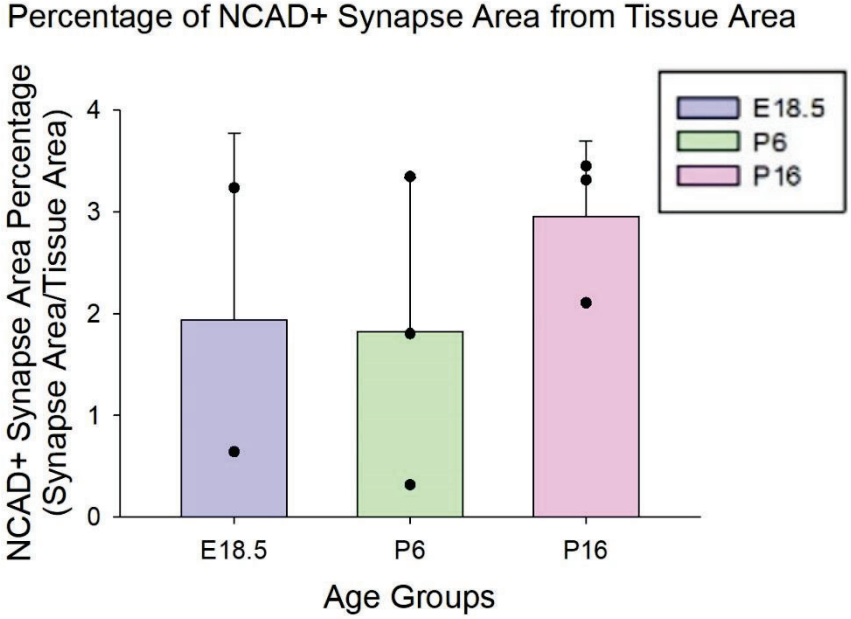

Figure 22, Percentage of NCAD+ Synapse Area from Tissue Area: N-Cadherin positive synapse area divided by tissue area in averaged biological replicates. Trend in data suggests that area occupied by synapses increases over time. Two biological replicates for E18.5, three for P6, and three for P16 with standard deviation included.

between each of the biological replicates (Fig. 21). Largest synapse size could be

observed at postnatal day 16 with low variation between all three biological replicate data points (Fig. 21).

The last bar graph depicts the percentage of N-Cadherin positive synapse area within the measured tissue area (Fig. 22). The largest N-Cadherin positive synapse area was observed at postnatal day 16 and the lowest synapse area at postnatal day 6 which is interesting due to the high density observed previously (Fig.21 & 22). Considerable variation was noticed in biological replicate data points at embryonic day 18.5 and postnatal day 6 (Fig. 22). T-Tests were used to discern differences between postnatal day 6 and postnatal day 16. A significant increase in N-Cadherin positive synapse size was detected by SigmPlot with a P-value of 0.0407. No significant differences were detected in N-Cadherin positive synapse density or area (P-value: 0.425 & 0.145).

Analysis of N-Cadherin Negative Synapses

The third aspect of this project examined differences in the N-Cadherin negative identified synapses. The first bar graph depicted N-Cadherin negative synapse density across time and the greatest density could be noticed at postnatal day 6 (Fig. 23). This trend is observed in all data pertaining to synapse density at this developmental time point (Figs. 19, 21, 23). There was no discernable difference between embryonic day 18.5 and postnatal day 16. The lowest individual data variation was seen at embryonic day 18.5 and the highest at postnatal day 6 (Fig. 23).

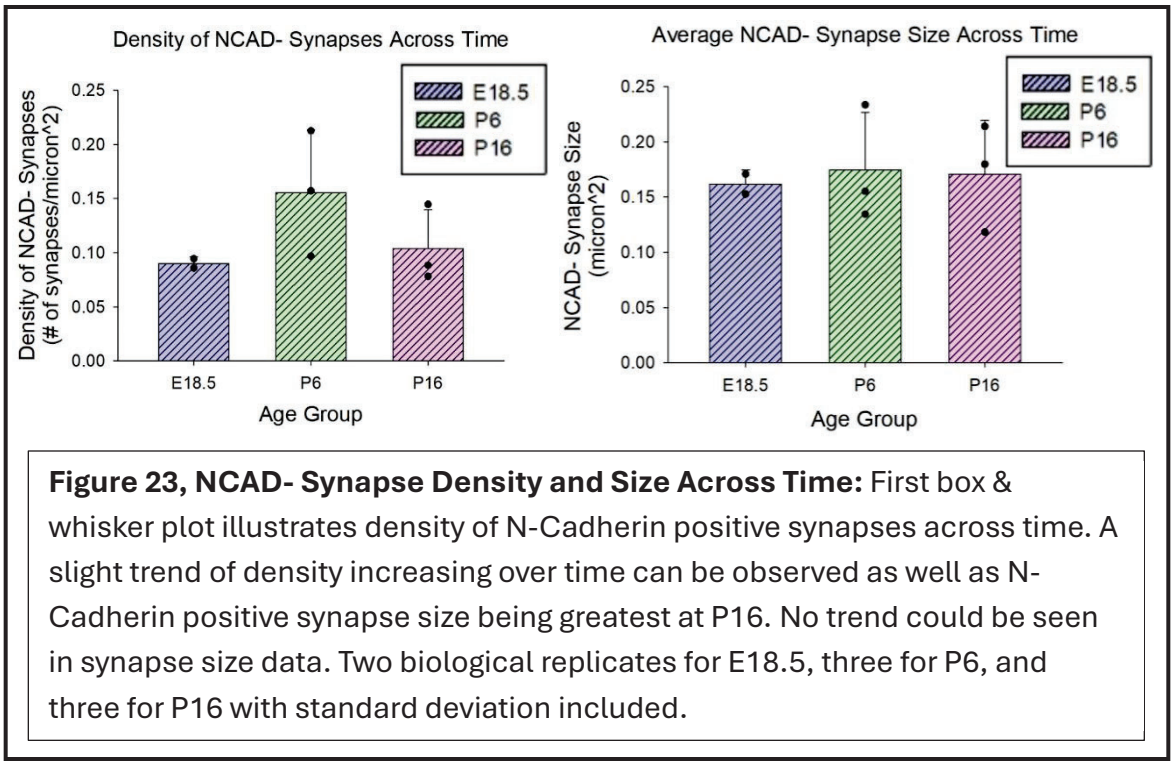

Figure 23, NCAD- Synapse Density and Size Across Time: First box & whisker plot illustrates density of N-Cadherin positive synapses across time. A slight trend of density increasing over time can be observed as well as N-Cadherin positive synapse size being greatest at P16. No trend could be seen in synapse size data. Two biological replicates for E18.5, three for P6, and three for P16 with standard deviation included.

The next bar graph depicts data of the average N-Cadherin negative synapse size from the biological replicates and the associated standard deviation. There was no discernable difference between the average N-Cadherin negative synapse size between any of the time points (Fig. 23). Variation between individual biological replicates did increase over time (Fig. 23).

Lastly, the N-Cadherin negative synapse area data was plotted into a bar graph, seen in Figure 24. Here the highest percentage of occupied synapse area was observed at postnatal day 6, as well as the greatest variation in individual biological replicate data points (Fig. 24). The lowest occupied area noticed at embryonic day 18.5, and it had the least variation within biological replicate data points (Fig. 24). T-Tests were implemented to detect significant differences between postnatal day 6 and

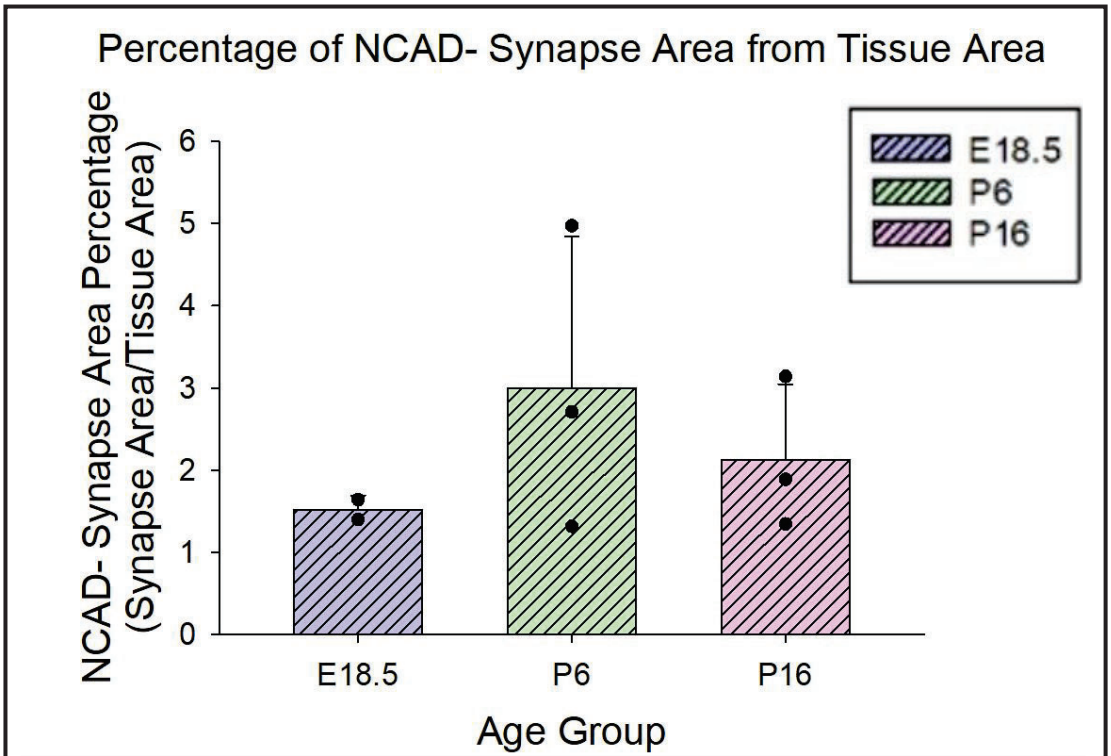

Figure 24, Percentage of NCAD- Synapses Area from Tissue Area: N-Cadherin negative Synapse area divided by the total tissue area. Largest N-Cadherin negative synapse area seen at P6 based on trending data. Two biological replicates for E18.5, three for P6, and three for P16 with standard deviation.

postnatal day 16. No significant differences were observed in N-Cadherin negative synapse density, size, or area between postnatal day 6 and postnatal day 16 (P-values: 0.129, 0.466, 0.252).

Two-Way ANOVA Analysis of Age Groups and Positive vs Negative N-Cadherin Synapses

The final graphical depictions of the results from the data gathered from immunofluorescence compared the two independent variables of the different ages groups and whether the synapses were positive or negative for N-Cadherin. The first graph, depicted in Figure 25, was used to determine the trends within the data for

synapse density. There was a slight increase in N-Cadherin negative synapses at embryonic day 18.5 but the high variation in individual biological replicate data negates

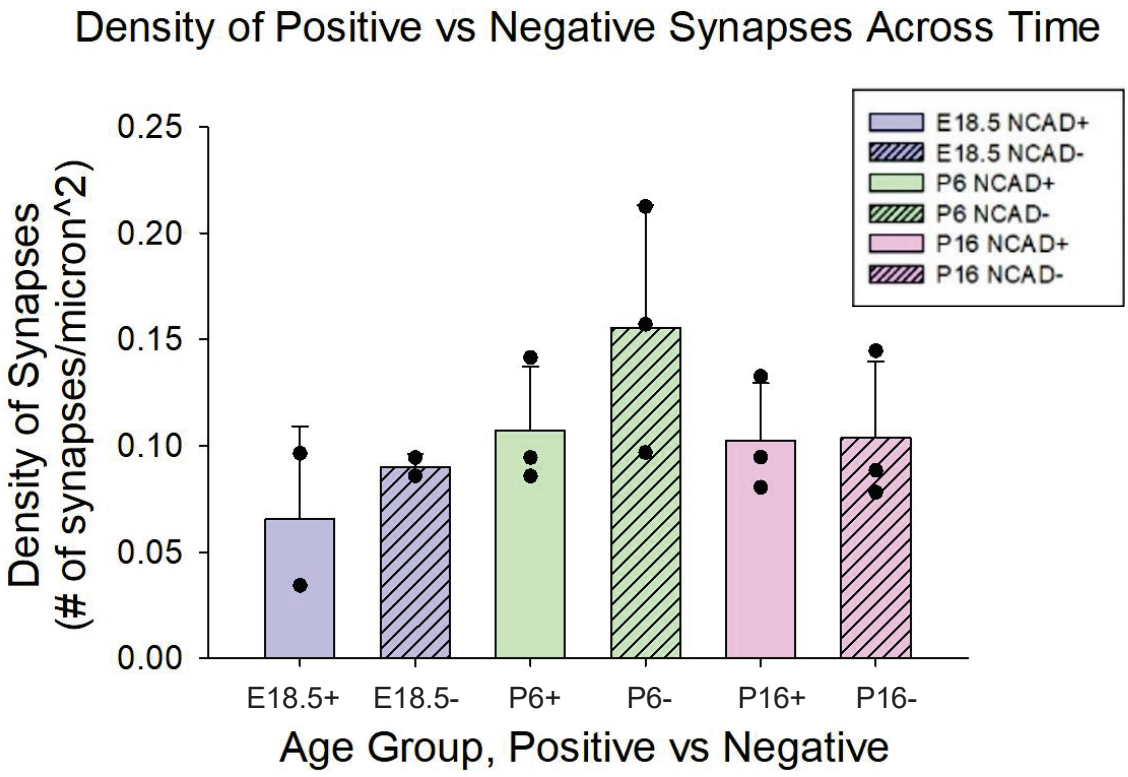

Figure 25, Comparison of Age & Synapse Group Across Time: Bar graph of normalized synapse number for both positive and negative synapses across age groups. Trends show greater amounts of N-Cadherin negative synapses and the greatest density at P6. Two biological replicates for E18.5, three for P6, and three for P16 with standard deviation.

any true difference between the N-Cadherin positive and N-Cadherin negative synapse density (Fig. 25). At postnatal day 6 there was an increase in N-Cadherin negative synapse density compared to N-Cadherin positive synapse density, with considerable variation in individual data points (Fig. 25). At postnatal day 16 there was no discernable difference between the N-Cadherin positive or N-Cadherin negative synapse density, and they had similar variation in individual data points (Fig. 25). The highest observable

density could be noticed at postnatal day 6 and the lowest at embryonic day 18.5 (Fig. 25).

The next bar graph examined trends in synapse size between the age groups and positive versus negative N-Cadherin synapses, depicted in Figure 26. Trends in the data suggest that N-Cadherin positive synapses were larger than the N-Cadherin negative synapses at each time point. At embryonic day 18.5 there was a large variation between the two biological replicate averages, as seen by the individual data points in

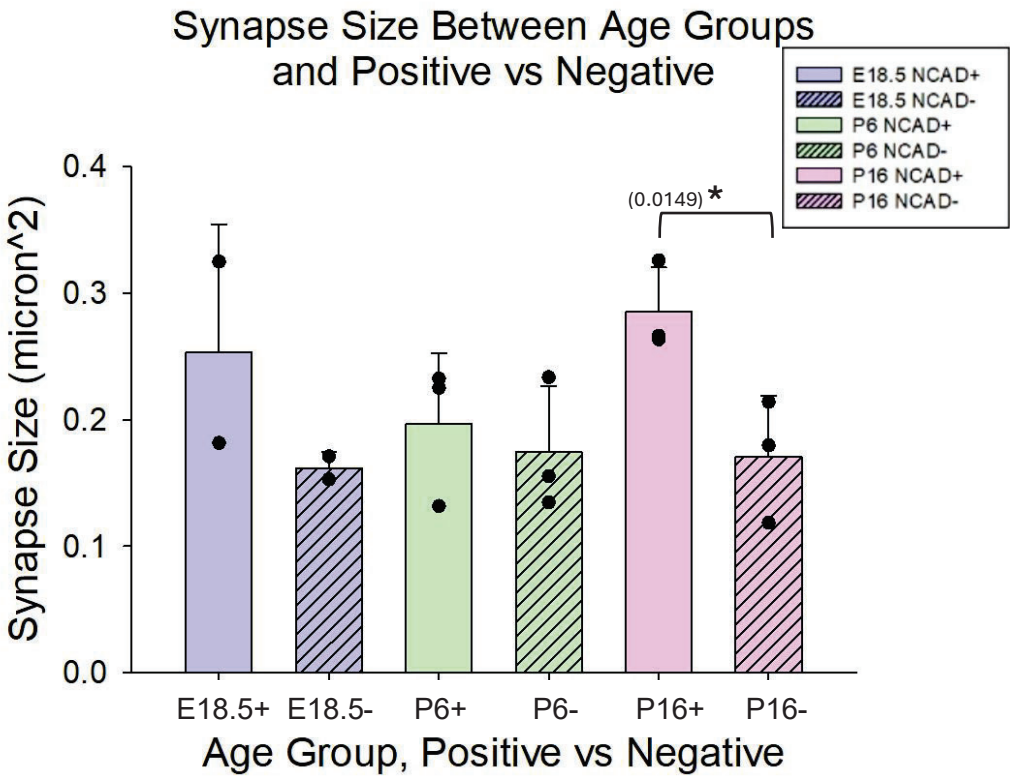

Figure 26, Comparison of Age Groups and Positive vs Negative Synapse Size: Bar graph depicting comparisons of the age groups with N-Cadherin positive and negative synapses. Trends in data suggest that the N-Cadherin positive synapses are larger in size on average than N-Cadherin negative synapses. T-test detected significance at P16 (P-value: 0.0149) Two biological replicates for E18.5, three for P6, and three for P16 with standard deviation.

Figure 26. The N-Cadherin positive synapses were on average larger than the negative synapses. At postnatal day 6 there was less of a difference between the N-Cadherin positive synapses and the N-Cadherin negative synapses, though there was still a larger average size in the positive synapses (Fig. 26). At postnatal day 16 there was a large difference between the N-Cadherin positive and N-Cadherin negative synapses, with the N-Cadherin positive synapses being larger (Fig. 26). There was also less variation in the postnatal day 16 individual biological replicates plot points than in the other age groups (Fig. 26). In summary, trends within the data suggest differences between the average N-Cadherin positive and N-Cadherin negative synapse size with the positive synapses being larger, and the largest synapse size occurring at postnatal day 16 (Fig. 26).

The last bar graph depicted the data associated with the occupied synapse area within the measured tissue area. Trends within the data suggest that there was little difference between the occupied area at any of the time points and there was high variability within the biological replicate data in each age group (Fig. 27). The largest percentage of area occupied was observed at postnatal day 6 in the N-Cadherin negative synapses. The differences in N-Cadherin positive versus N-Cadherin negative synapses also varied between the time points, preventing trends from being discerned within the data. T-tests were implanted to discern differences between N-Cadherin positive synapses and N-Cadherin negative synapses within the age groups of postnatal day 6 and postnatal day 16. The only significant difference detected was at postnatal day 16 in that the size of the N-Cadherin positive synapses were statistically larger than the N-Cadherin negative synapses with an associated P-value of 0.0149. No

differences between N-Cadherin positive or N-Cadherin negative synapses density or area were detected at postnatal day 16 (P-value: 0.483 & 0.145). No significant differences between N-Cadherin positive or negative synapse density, size, or area at postnatal day 6 were observed (P-value: 0.135, 0.323, & 0.221).

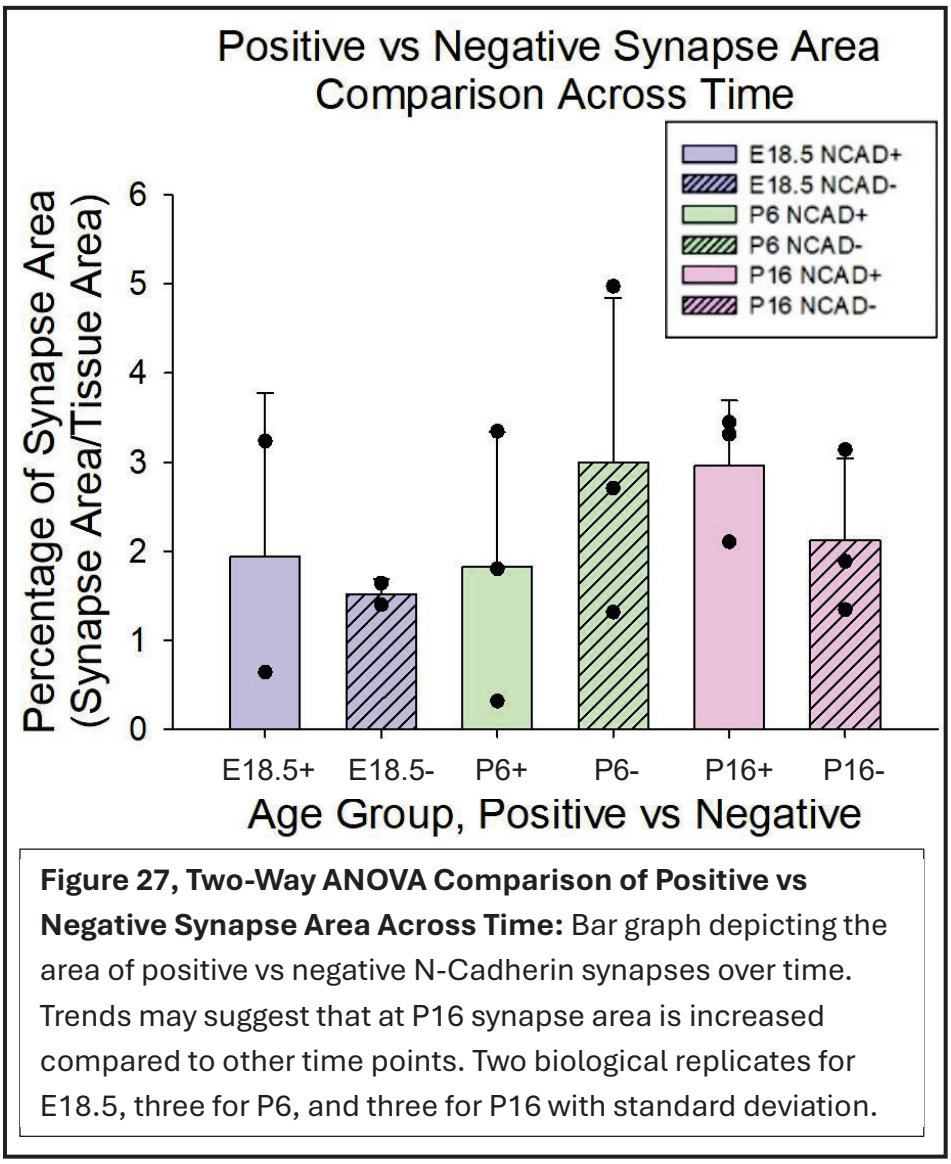

Figure 27, Two-Way ANOVA Comparison of Positive vs Negative Synapse Area Across Time: Bar graph depicting the area of positive vs negative N-Cadherin synapses over time. Trends may suggest that at P16 synapse area is increased compared to other time points. Two biological replicates for E18.5, three for P6, and three for P16 with standard deviation.

CHAPTER 4

DISCUSSION

Golgi-Cox Staining Conclusions:

Our purpose was to optimize techniques to investigate how dendritic spines are affected throughout all stages of life in ASD brain tissue samples. To accomplish this, we had to optimize Golgi staining and immunofluorescence in mice brain tissue first before being granted access to the ASD tissue samples in the future. We started with the optimization of Golgi staining. Our first experiment utilized the Golgi-Kopsh technique on control human brain tissue, but there was not adequate staining of the dendritic spines (Fig. 8). Mouse brain tissue was then utilized as it was a more readily available resource, and we moved onto using the Golgi-Cox technique as well. This change in technique proved to be successful for ensuring the dendritic spines were stained properly (Fig. 9). The change allowed us to accurately identify dendritic spine morphology and number. Unfortunately, there was visual obstruction by astrocytes over the soma and dendrite branches (Fig. 9). The solution was to remove the prefixing of the tissue in formaldehyde; this ameliorated the preferential staining of the astrocytes over neurons (Fig. 13). The cause for the preference of astrocytes is not known, but there are a few older papers that have documented this phenomenon[70]. Ranjan and Mallik in 2012 investigated the intricacies of prefixing in rat brains and the effects it could have when Golgi staining was done[71]. They concluded that perfusion with 4% paraformaldehyde or formalin caused preferential glia staining even if the brain tissue had been washed with PBS first before the perfusion[71]. This was also noted when there was fixative used during the staining process as well[71]. Interestingly, exposing tissue to

microwaves also produced preferential glia staining[70]. The staining of astrocytes can be a negative when researchers are focused on studying neurons, but it can be beneficial for those wishing to research protoplasmic astrocytes, fibrous astrocytes, and oligodendrocytes. Staining of microglia was not found to be prevalent however, which would have been helpful when investigating disorders such as multiple sclerosis or Alzheimer's Disease. In our study we removed prefixing with 4% formaldehyde from our protocol as potassium dichromate could be used as fixative[73]. Potassium dichromate binds to lipids for fixation and 50% of the brain's dry weight is attributed to lipids[74]. With the preferential staining ameliorated and knowing that one of our essential chemicals can fix brain tissue we were able to proceed with our optimization of Golgi-Cox staining in mice brains. We combined our improved protocol with the Neurolucida program to accurately trace the neuron and identify the dendritic spine morphology and quantify the number of spines per neuron. Our future plans include the use of these techniques to investigate what are the prominent types of dendritic spines that are present in the varying timepoints through life in ASD. We would like to also utilize immunofluorescence in parallel with this protocol so that we may identify what adhesions proteins are predominant in the different dendritic spine morphologies.

Immunofluorescence Conclusions:

The next goal was to adjust IF protocols for future use so that we could investigate what adhesion proteins are present in synapses across developmental stages, and how these are altered in the presence of ASD-associated genetic mutations and/or environmental factors. To accomplish this, we investigated the presence of N-Cadherin during early developmental time points in mice, as N-Cadherin is a protein

associated with synapse formation and maturation. Our hypothesis was that as synapse development progresses there would be increased localization of N-Cadherin to synapses over time. The results of the investigation were inconclusive due to the low sample power impeding the detection of significant differences in the statistical analysis process. However certain trends could be observed within the data. Our starting point was embryonic day 18.5 as it is the period of mice development where synaptogenesis begins[75]. It was at this time point that we observed the lowest density of synapse compared to postnatal day 6 or 16. At time point postnatal day 6, it is the peak of synapse formation in mice, our results potentially showed trends that at postnatal day 6 there was increased synapse density compared to our other two time points (Fig. 19)[75]. At postnatal day 16 we observed a decrease in synapse number as weaker synapses are pruned while others are beginning to mature and strengthen. The overall results of synaptic density were inconclusive due to the low power of the sample size which did not allow use to perform any statistical analysis, instead bar graphs were used to discern trends within the data. We compared the observations made about synapse density to the area occupied by N-Cadherin positive synapses detected in the tissue samples. There was an increase of area between time points embryonic day 18.5 and postnatal day 16 (Fig. 20). This inverse of having decreased number synapses but occupying a greater area implies that the synapses are getting larger over time. The literature supports a role for N-Cadherin in facilitating synapse stabilization and maturation, which leads to dendritic spine head expansion[48,49,57–59,76]. Furthermore, between postnatal day 6 and postnatal day 16, we observed a significant increase in the size of N-Cadherin-positive synapses, but not N-Cadherin-negative synapses (Fig. 21 &

23). This was later confirmed by a T-test which detected a significant increase in N-Cadherin positive synapse size from postnatal day 6 to postnatal day 16 (P-value: 0.0407). Previous literature has identified that N-Cadherin is involved more in synapse maturation than formation, which includes the lateral expansion of the dendritic spine head[48,49,76]. This lateral expansion would cause the synapse to increase in size and this is supported by trends in our data that as the mouse brain develops there is an increase in size of N-Cadherin positive synapses. When we investigated the characteristics of N-Cadherin negative synapses, we did not see a change in the density of negative synapses detected, nor did we see a change in negative synapse size over time (Fig. 23). As stated previously, it is during the second and third weeks of postnatal development in mice that synapses are maturing and expanding[74]. Trends in our data are supported by previous literature, suggesting that N-Cadherin is involved more in synapse maturation than formation[48,49]. Synapse maturation includes the lateral expansion of the dendritic spine head[26]. This lateral expansion increases the pre- and post-synaptic contact area, as observed specifically for N-Cadherin positive synapses (Fig. 21 & 22). These trends in our indicate a role for other adhesion proteins in synapse formation and maturation, not just N-Cadherin. When looking at Figure 23 there was a large range in N-Cadherin negative synapse size, showing a diverse array of synapse size. We do know from past research that other adhesion molecules such as neuroligin-1 and synCAM1 have similar roles to N-Cadherin in synapse stabilization and maturation[11,33,47,51–53,77–79]. When we compared the density of synapses of positive versus negative synapses over time, we observed an increase of synapse density at postnatal day 6 and a slight difference between positive versus negative N-Cadherin

synapses at the same point (Fig. 25). Trends which could be noticed in the data though suggest that synapse density increases over time and that there was a difference in positive N-Cadherin synapses versus N-Cadherin negative synapses. The second two independent variable bar graph examined the differences in N-Cadherin positive versus N-Cadherin negative synapse size over time (Fig. 26). In this graph we discerned a difference in synapses size over time and a difference between the positive vs negative synapses (Fig 26). There was also an observable difference in N-Cadherin positive synapse size versus N-Cadherin negative synapses, with a T-Test confirming the difference at postnatal day 16 (P-value: 0.0149). It could be observed that there was a decrease in N-Cadherin negative synapse area at postnatal day 6 even though in previous graphs observations have the highest synapse density at postnatal day 6 (Fig. 25 & 27). The results of this investigation support the idea that N-Cadherin plays a role in synapse maturation and stabilization[48,49,76]. We observed that N-Cadherin positive synapses were larger in size than N-Cadherin negative synapses, supporting the role of N-Cadherin in dendritic spine morphogenesis or the lateral expansion of the spine head[48,49,76]. There was a change in N-Cadherin positive synapse size between postnatal day 6 and postnatal day 16, further supporting the idea that it is N-Cadherin which is essential for lateral head expansion. We also saw this increase in N-Cadherin positive synapse size occur from postnatal day 6 to postnatal day 16. These results reflect the conclusions made in previous investigations which looked at the role N-Cadherin had in synapse maturation and stabilization through affecting its associated proteins in the Cadherin-Catenin complex, causing deficits in the dendritic spine head morphology[49,61]. Another result of our data supports these implications when at postnatal day 6 it could

be seen that there was a high density of synapses but a low area occupied by synapses, highlighting that the N-Cadherin negative synapses were smaller (Fig. 25 & 27). This was a significant finding to us because it shows that even though there was a higher density of synapses at postnatal day 6 these synapses were smaller and occupied less area than at postnatal day 16 where there were less synapses (Fig. 25 & 27). It is our goal to expand this methodology to human brain tissue samples to investigate how dendritic spines are affected throughout life in both neurotypical and ASD brain tissue. We wish to investigate not only N-Cadherin but neuroligin-1 and synCAM1 as well. These are all important adhesion proteins that already have implications in the development of ASD and could also be affected by time, contributing to the increased likelihood of developing Alzheimer's Disease in ASD individuals[7,47,51,78,80]. Using human brain tissue is not the only way to investigate dendritic spines and synapses and we would also like to expand our experimental methods to include human stem cell culture research to investigate the roles of the specified adhesion proteins in the initial stages of synapses formation[81].

Future Expanded Investigations Into Adhesion Proteins:

SynCAM1 and neuroligin-1 are two other proteins with similar roles and implications in ASD development to N-Cadherin[33,47,51,53,77,78,82]. It is our intent in the future to investigate the role of these adhesion proteins in synapse formation, along with N-Cadherin. In this study we used post-mortem tissue to study neurons but there are other models widely used to investigate neurons and their connections. Human derived induced pluripotent stem cells (hIPCS) are used in neuronal cell cultures and can be derived from those affected by a particular disorder[17]. One of our proposed investigative

experiments is to utilize microfluidic devices (MFDs) and hIPCS to observe the initial stages of synaptogenesis. These devices allow researchers to organize synapse development to provide a clearer visualization of the initial contact between the pre- and post-synaptic membrane[81]. In neuronal cell cultures the formation of synapses can be chaotic and difficult to identify due to the tangled web of axons and dendrite branches. The MFDs have microchannels along the center of the device to allow individual axons and dendrites to enter and form a connection[81]. These channels can then be viewed under a microscope in an organized manner that makes the study of them easier[81]. We would like to use these devices to study what happens if either N-Cadherin, neuroligin-1, or synCAM1 are knocked out in human neural progenitor cells. We can then potentially elucidate their roles in the initial stages of synapse formation, an under researched area due to a lack of tools to observe the phenomenon.

Neural Inflammation Connections Between ASD & Alzheimer's Disease:

Similar to our reasons for studying N-Cadherin, the genes encoding for neuroligin-1 and synCAM1, when perturbed are risk factors for developing ASD[7,9,10]. One postulation is that mutations to synaptic adhesion protein genes can cause the expressed proteins to be more susceptible to damage from stressors such as oxidative stress and neural inflammation. Oxidative stress and neural inflammation are seen in higher levels than found in neurotypicals, leading it to be a topic of interest for current researchers investigating ASD. Oxidative stress occurs when there is an imbalance in the antioxidant to oxidant ratio that leads to a disruption in the redox signaling potentially causing damage to the surrounding cellular environment[83]. Inflammation is a protective mechanism allowing the immune system to recognize and remove stimuli

which can be harmful to the body[84]. Neural inflammation are chronic glia mediated reactions that do not always exhibit the same characteristics as peripheral inflammation[85]. This phenomena can cause brain tissue damage over time when chronic and has been implicated in neurodegenerative and neuropsychiatric diseases[7,8,85–88]. Our curiosity stems from the correlations between ASD and Alzheimer's Disease that could be related to the increased prevalence of developing early onset Alzheimer's Disease when the individual already has ASD. As stated in the introduction of this paper, those diagnosed with ASD have a fourfold increase in developing early onset Alzheimer's Disease[1]. Both conditions see increased amounts of systemic inflammation[7,87–89]. In ASD, there are chronically high levels of activated B-cells, NK cells, and proinflammatory cytokines in the peripheral immune system[7]. When there is chronic inflammation in the body it creates negative effects on area's such as the brain or gastrointestinal tract[86]. Gastrointestinal issues are often comorbid with ASD diagnosis', and experience chronically high levels of proinflammatory markers such as TNF-α[86,90,91]. When microglia, the resident immune cell in the brain, are activated to enter their proinflammatory state they produce transcription factors for proinflammatory cytokines such as interleukin factor 6 (IL-6) and tumor necrosis factor alpha (TNF-α)[90]. These observations conclude that those with ASD experience chronic levels of inflammation that possibly affect the brain as well. Inflammation is a predominant marker in ASD and Alzheimer's Disease, and we know that chronically high levels of inflammation can lead to tissue damage. This could potentially be the connection between ASD patients developing early onset Alzheimer's Disease. Our next section will postulate possible metabolic connections between Alzheimer's Disease and ASD.

Metabolic Connections between ASD and Alzheimer's Disease:

Despite increased spine density in ASD adolescents, ASD risk factors may contribute to early synaptic loss leading to Alzheimer's disease. Disturbances in cell metabolism is a proposed phenotype for ASD, where the disturbances can create molecules that damage the surrounding cell components and cellular environment[89,92]. These metabolic issues lead to increased levels of reactive oxygen species (ROSs) and mitochondrial related apoptosis[89]. ROSs are also present in Alzheimer's Disease, as mitochondrial dysfunction is a proposed theory of the pathology behind the illness[93]. ROSs can be harmful when there are higher than normal levels and cannot be properly regulated leading to harm across many components inside a cell[83,92]. Similar with inflammation, the adhesion proteins could be more susceptible to damage from these ROSs, or the overall increased amount is naturally more destructive over time, leading to the increase in prevalence of early onset Alzheimer's Disease. The harm to the adhesion proteins caused by inflammation and/or oxidative stress could possibly be leading to the degradation of synapses by destroying the connection between the pre- and post-synaptic membrane or destabilizing the proteins necessary for supporting the dendritic spines. These questions create a need for more investigations into how adhesion proteins in synapses are affected over time as well as their effects on the integrity of dendritic spines. The lack of understanding behind the pathology of both ASD and Alzheimer's Disease has led us and other researchers to create and optimize methods for investigating these questions.

Our goal in this project was to optimize techniques for investigating dendritic spine morphologies over the human lifetime and the synaptic adhesion proteins

associated with their formation, maturation, and stabilization. The conclusion from our immunofluorescence was that there is an association between N-Cadherin and maturation of synapses as we detected increases in N-Cadherin positive synapse size from postnatal day 6 to postnatal day 7. We also saw a difference in N-Cadherin positive synapse size versus N-Cadherin negative synapse size at postnatal day 16. The last observation we could see in this study was that there was a reduction in N-Cadherin negative synapse area at postnatal day 6 even though there had been a high density observed previously, highlighting how N-Cadherin negative synapses are smaller than the N-Cadherin positive synapses as their area increased from postnatal day 6 to postnatal day 16. This supports previous studies which have investigated the roles N-Cadherin has in synapses in early neural development[48,49,61,76]. Our future goal is to use the technique we optimized in this study and apply it to later in life ASD brain tissue samples to investigate the density and morphology of the dendritic spines as well as what adhesion molecules are present in the synapses during all stages in human development and life.

References

1. Maenner, M. J. *et al.* Prevalence and Characteristics of Autism Spectrum Disorder Among Children Aged 8 Years — Autism and Developmental Disabilities Monitoring Network, 11 Sites, United States, 2020. *MMWR Surveill. Summ.* **72**, 1–14 (2023).

2. Bailey, A. A clinicopathological study of autism. *Brain* **121**, 889–905 (1998).

3. Fombonne, E. Epidemiology of Pervasive Developmental Disorders. *Pediatr. Res.* **65**, 591–598 (2009).

4. Hirota, T. & King, B. H. Autism Spectrum Disorder: A Review. *JAMA* **329**, 157 (2023).

5. *Diagnostic Statistical Manual for Mental Disorders*. (American Psychiatric Association, 2013).

6. Hyman, S. L. *et al.* Executive Summary: Identification, Evaluation, and Management of Children With Autism Spectrum Disorder. *Pediatrics* **145**, e20193448 (2020).

7. Chaste, P. & Leboyer, M. Autism risk factors: genes, environment, and gene-environment interactions. *Dialogues Clin. Neurosci.* **14**, 281–292 (2012).

8. Taleb, A. *et al.* Emerging mechanisms of valproic acid-induced neurotoxic events in autism and its implications for pharmacological treatment. *Biomed. Pharmacother.* **137**, 111322 (2021).

9. Varghese, M. *et al.* Autism spectrum disorder: Neuropathology and animal models. *Acta Neuropathol. (Berl.)* **134**, 537–566 (2017).

10. Genovese, A. & Butler, M. G. Clinical Assessment, Genetics, and Treatment Approaches in Autism Spectrum Disorder (ASD). *Int. J. Mol. Sci.* **21**, 4726 (2020).

11. Zhiling, Y. *et al.* Mutations in the gene encoding CADM1 are associated with autism spectrum disorder. *Biochem. Biophys. Res. Commun.* **377**, 926–929 (2008).

12. Yasuda, S. *et al.* Activity-Induced Protocadherin Arcadlin Regulates Dendritic Spine Number by Triggering N-Cadherin Endocytosis via TAO2β and p38 MAP Kinases. *Neuron* **56**, 456–471 (2007).

13. Villa, K. L. & Nedivi, E. Excitatory and Inhibitory Synaptic Placement and Functional Implications. in *Dendrites* (eds. Emoto, K., Wong, R., Huang, E. & Hoogenraad, C.) 467–487 (Springer Japan, Tokyo, 2016). doi:10.1007/978-4-431-56050-0_18.

14. Hutsler, J. J. & Zhang, H. Increased dendritic spine densities on cortical projection neurons in autism spectrum disorders. *Brain Res.* **1309**, 83–94 (2010).

15. Zhan, Y. *et al*. Deficient neuron-microglia signaling results in impaired functional brain connectivity and social behavior. *Nat. Neurosci.* **17**, 400–406 (2014).

16. Papariello, A., Taylor, D., Soderstrom, K. & Litwa, K. CB1 antagonism increases excitatory synaptogenesis in a cortical spheroid model of fetal brain development. *Sci. Rep.* **11**, 9356 (2021).

17. Papariello, A. & Newell-Litwa, K. Human-Derived Brain Models: Windows into Neuropsychiatric Disorders and Drug Therapies. *ASSAY Drug Dev. Technol.* **18**, 79–88 (2020).

18. Vivanti, G., Tao, S., Lyall, K., Robins, D. L. & Shea, L. L. The prevalence and incidence of early-onset dementia among adults with autism spectrum disorder. *Autism Res.* **14**, 2189–2199 (2021).

19. Tang, G. *et al*. Loss of mTOR-Dependent Macroautophagy Causes Autistic-like Synaptic Pruning Deficits. *Neuron* **83**, 1131–1143 (2014).

20. Mijalkov, M. *et al*. Dendritic spines are lost in clusters in Alzheimer's disease. *Sci. Rep.* **11**, 12350 (2021).

21. Boros, B. D., Greathouse, K. M., Gearing, M. & Herskowitz, J. H. Dendritic spine remodeling accompanies Alzheimer's disease pathology and genetic susceptibility in cognitively normal aging. *Neurobiol. Aging* **73**, 92–103 (2019).

22. Penzes, P., Cahill, M. E., Jones, K. A., VanLeeuwen, J.-E. & Woolfrey, K. M. Dendritic spine pathology in neuropsychiatric disorders. *Nat. Neurosci.* **14**, 285–293 (2011).

23. Walker, C. K. & Herskowitz, J. H. Dendritic Spines: Mediators of Cognitive Resilience in Aging and Alzheimer's Disease. *Neurosci. Rev. J. Bringing Neurobiol. Neurol. Psychiatry* **27**, 487–505 (2021).

24. Synaptic Impairment in Alzheimer's Disease: A Dysregulated Symphony - ClinicalKey. https://www.clinicalkey.com/#!/content/playContent/1-s2.0-S0166223617300693?returnurl=https:%2F%2Flinkinghub.elsevier.com%2Fretrieve%2Fpii%2FS0166223617300693%3Fshowall%3Dtrue&referrer=https:%2F%2Fpubmed.ncbi.nlm.nih.gov%2F.

25. Raghavan, M., Fee, D. & Barkhaus, P. E. Generation and propagation of the action potential. in *Handbook of Clinical Neurology* vol. 160 3–22 (Elsevier, 2019).

26. Holtmaat, A. & Svoboda, K. Experience-dependent structural synaptic plasticity in the mammalian brain. *Nat. Rev. Neurosci.* **10**, 647–658 (2009).

27. Yuste, R. & Bonhoeffer, T. Genesis of dendritic spines: insights from ultrastructural and imaging studies. *Nat. Rev. Neurosci.* **5**, 24–34 (2004).

28. Brennand, K. J. *et al.* Modelling schizophrenia using human induced pluripotent stem cells. *Nature* **473**, 221–225 (2011).

29. Glantz, L. A. & Lewis, D. A. Decreased Dendritic Spine Density on Prefrontal Cortical Pyramidal Neurons in Schizophrenia. *Arch. Gen. Psychiatry* **57**, 65–73 (2000).

30. Vaughn, J. E. Review: Fine structure of synaptogenesis in the vertebrate central nervous system. *Synapse* **3**, 255–285 (1989).

31. Dailey, M. E. & Smith, S. J. The Dynamics of Dendritic Structure in Developing Hippocampal Slices. *J. Neurosci.* **16**, 2983–2994 (1996).

32. Peters, A. & Kaiserman-Abramof, I. R. The small pyramidal neuron of the rat cerebral cortex. The perikaryon, dendrites and spines. *Am. J. Anat.* **127**, 321–355 (1970).

33. Körber, N. & Stein, V. In vivo imaging demonstrates dendritic spine stabilization by SynCAM 1. *Sci. Rep.* **6**, (2016).

34. Iasevoli, F., Tomasetti, C. & de Bartolomeis, A. Scaffolding Proteins of the Post-synaptic Density Contribute to Synaptic Plasticity by Regulating Receptor Localization and Distribution: Relevance for Neuropsychiatric Diseases. *Neurochem. Res.* **38**, 1–22 (2013).

35. Jung, S. & Park, M. Shank postsynaptic scaffolding proteins in autism spectrum disorder: Mouse models and their dysfunctions in behaviors, synapses, and molecules. *Pharmacol. Res.* **182**, 106340 (2022).

36. Gao, L. *et al.* Shank promotes action potential repolarization by recruiting BK channels to calcium microdomains. *eLife* **11**, e75140.

37. Gu, J., Firestein, B. L. & Zheng, J. Q. Microtubules in Dendritic Spine Development. *J. Neurosci.* **28**, 12120–12124 (2008).

38. Suzuki, T., Kametani, K., Guo, W. & Li, W. Protein components of post-synaptic density lattice, a backbone structure for type I excitatory synapses. *J. Neurochem.* **144**, 390–407 (2018).

39. Matus, A., Ackermann, M., Pehling, G., Byers, H. R. & Fujiwara, K. High actin concentrations in brain dendritic spines and postsynaptic densities. *Proc. Natl. Acad. Sci. U. S. A.* **79**, 7590–7594 (1982).

40. Okamoto, K.-I., Nagai, T., Miyawaki, A. & Hayashi, Y. Rapid and persistent modulation of actin dynamics regulates postsynaptic reorganization underlying bidirectional plasticity. *Nat. Neurosci.* **7**, 1104–1112 (2004).

41. Fukazawa, Y. *et al.* Hippocampal LTP Is Accompanied by Enhanced F-Actin Content within the Dendritic Spine that Is Essential for Late LTP Maintenance In Vivo. *Neuron* **38**, 447–460 (2003).

42. Hu, X., Viesselmann, C., Nam, S., Merriam, E. & Dent, E. W. Activity-Dependent Dynamic Microtubule Invasion of Dendritic Spines. *J. Neurosci.* **28**, 13094–13105 (2008).

43. Faust, T., Gunner, G. & Schafer, D. P. Mechanisms governing activity-dependent synaptic pruning in the mammalian CNS. *Nat. Rev. Neurosci.* **22**, 657–673 (2021).

44. Qi, C., Luo, L.-D., Feng, I. & Ma, S. Molecular mechanisms of synaptogenesis. *Front. Synaptic Neurosci.* **14**, 939793 (2022).

45. Lüscher, C. & Malenka, R. C. NMDA Receptor-Dependent Long-Term Potentiation and Long-Term Depression (LTP/LTD). *Cold Spring Harb. Perspect. Biol.* **4**, a005710 (2012).

46. von Bernhardi, R., Bernhardi, L. E. & Eugenín, J. What Is Neural Plasticity? in *The Plastic Brain* (eds. von Bernhardi, R., Eugenín, J. & Muller, K. J.) 1–15 (Springer International Publishing, Cham, 2017). doi:10.1007/978-3-319-62817-2_1.

47. Robbins, E. M. *et al.* SynCAM 1 Adhesion Dynamically Regulates Synapse Number and Impacts Plasticity and Learning. *Neuron* **68**, 894–906 (2010).

48. Okamura, K. *et al.* Cadherin activity is required for activity-induced spine remodeling. *J. Cell Biol.* **167**, 961–972 (2004).

49. Togashi, H. *et al.* Cadherin Regulates Dendritic Spine Morphogenesis. *Neuron* **35**, 77–89 (2002).

50. Newell-Litwa, K. A. Breaking down to build up: Neuroligin's C-terminal domain strengthens the synapse. *J. Cell Biol.* **212**, 375–377 (2016).

51. de Arce, K. P. *et al.* Concerted roles of LRRTM1 and SynCAM 1 in organizing prefrontal cortex synapses and cognitive functions. *Nat. Commun.* **14**, 459 (2023).

52. Kwon, H.-B. *et al.* Cortical synaptogenesis and excitatory synapse number are determined via a Neuroligin-1-dependent intercellular competition. *Nat. Neurosci.* **15**, 1667–1674 (2012).

53. Giannone, G. *et al.* Neurexin-1β Binding to Neuroligin-1 Triggers the Preferential Recruitment of PSD-95 versus Gephyrin through Tyrosine Phosphorylation of Neuroligin-1. *Cell Rep.* **3**, 1996–2007 (2013).

54. Neale, B. M. *et al.* Patterns and rates of exonic de novo mutations in autism spectrum disorders. *Nature* **485**, 242–245 (2012).

55. Israely, I. *et al.* Deletion of the Neuron-Specific Protein Delta-Catenin Leads to Severe Cognitive and Synaptic Dysfunction. *Curr. Biol.* **14**, 1657–1663 (2004).

56. Hofmeister, W. *et al. CTNND2* —a candidate gene for reading problems and mild intellectual disability. *J. Med. Genet.* **52**, 111–122 (2015).

57. Tsai, N.-P. & Huber, K. M. Protocadherins and the social brain. *Biol. Psychiatry* **81**, 173–174 (2017).

58. Cadherins in early neural development | Cellular and Molecular Life Sciences. https://link.springer.com/article/10.1007/s00018-021-03815-9.

59. Jontes, J. D. The Cadherin Superfamily in Neural Circuit Assembly. *Cold Spring Harb. Perspect. Biol.* **10**, a029306 (2018).

60. Bozdagi, O., Valcin, M., Poskanzer, K., Tanaka, H. & Benson, D. L. Temporally Distinct Demands for Classic Cadherins in Synapse Formation and Maturation. *Mol. Cell. Neurosci.* **27**, 509–521 (2004).

61. Okuda, T., Yu, L. M. Y., Cingolani, L. A., Kemler, R. & Goda, Y. β-Catenin regulates excitatory postsynaptic strength at hippocampal synapses. *Proc. Natl. Acad. Sci. U. S. A.* **104**, 13479–13484 (2007).

62. Learned helplessness: unique features and translational value of a cognitive depression model | Cell and Tissue Research. https://link.springer.com/article/10.1007/s00441-013-1654-2.

63. White, S. W. *et al.* Psychosocial treatments targeting anxiety and depression in adolescents and adults with autism spectrum disorder: Review of the latest research and recommended future directions. *Curr. Psychiatry Rep.* **20**, 82 (2018).

64. Ryu, T. *et al.* Improved memory and reduced anxiety in δ-catenin transgenic mice. *Exp. Neurol.* **318**, 22–31 (2019).

65. Forbes, M. S. Chapter 5 - Cell Structure. in *Cell Physiology Source Book (Fourth Edition)* (ed. Sperelakis, N.) 67–83 (Academic Press, San Diego, 2012). doi:10.1016/B978-0-12-387738-3.00005-6.

66. Bentivoglio, M. Ramón y Cajal, Santiago. in *Encyclopedia of the Neurological Sciences* (eds. Aminoff, M. J. & Daroff, R. B.) 130–132 (Academic Press, New York, 2003). doi:10.1016/B0-12-226870-9/01275-2.

67. The Nobel Prize in Physiology or Medicine 1906. *NobelPrize.org* https://www.nobelprize.org/prizes/medicine/1906/speedread/.

68. Cox, W. H. Imprägnation des centralen Nervensystems mit Quecksilbersalzen. *Arch. Für Mikrosk. Anat.* **37**, 16–21 (1891).

69. VL_BMK-2202_UserGuide_LBL02254.pdf.

70. Zhang, H., Weng, S.-J. & Hutsler, J. J. Does microwaving enhance the Golgi methods? A quantitative analysis of disparate staining patterns in the cerebral cortex. *J. Neurosci. Methods* **124**, 145–155 (2003).

71. Ranjan, A. & Mallick, B. N. Differential staining of glia and neurons by modified Golgi-Cox method. *J. Neurosci. Methods* **209**, 269–279 (2012).

72. Zhong, F., Liu, L., Wei, J.-L. & Dai, R.-P. Step by Step Golgi-Cox Staining for Cryosection. *Front. Neuroanat.* **13**, (2019).

73. Sharma, A. K. & Sharma, A. 3 - Fixation. in *Chromosome Techniques (Third Edition)* (eds. Sharma, A. K. & Sharma, A.) 30–70 (Butterworth-Heinemann, 1980). doi:10.1016/B978-0-408-70942-2.50008-0.

74. Yoon, J. H. *et al.* Brain lipidomics: From functional landscape to clinical significance. *Sci. Adv.* **8**, eadc9317.

75. Semple, B. D., Blomgren, K., Gimlin, K., Ferriero, D. M. & Noble-Haeusslein, L. J. Brain development in rodents and humans: Identifying benchmarks of maturation and vulnerability to injury across species. *Prog. Neurobiol.* **0**, 1–16 (2013).

76. Jüngling, K. *et al.* N-Cadherin Transsynaptically Regulates Short-Term Plasticity at Glutamatergic Synapses in Embryonic Stem Cell-Derived Neurons. *J. Neurosci.* **26**, 6968–6978 (2006).

77. Liu, A. *et al.* Neuroligin 1 regulates spines and synaptic plasticity via LIMK1/cofilin-mediated actin reorganization. *J. Cell Biol.* **212**, 449–463 (2016).

78. Chmielewska, J. J., Kuzniewska, B., Milek, J., Urbanska, K. & Dziembowska, M. Neuroligin 1, 2, and 3 Regulation at the Synapse: FMRP-Dependent Translation and Activity-Induced Proteolytic Cleavage. *Mol. Neurobiol.* **56**, 2741–2759 (2019).

79. Dahlhaus, R. *et al.* Overexpression of the cell adhesion protein neuroligin-1 induces learning deficits and impairs synaptic plasticity by altering the ratio of excitation to inhibition in the hippocampus. *Hippocampus* **20**, 305–322 (2010).

80. Blundell, J. *et al.* Neuroligin-1 Deletion Results in Impaired Spatial Memory and Increased Repetitive Behavior. *J. Neurosci.* **30**, 2115–2129 (2010).

81. Taylor, A. M., Dieterich, D. C., Ito, H. T., Kim, S. A. & Schuman, E. M. Microfluidic Local Perfusion Chambers for the Visualization and Manipulation of Synapses. *Neuron* **66**, 57–68 (2010).

82. Fogel, A. I. & Biederer, T. SynCAMs. in *Encyclopedia of Neuroscience* (ed. Squire, L. R.) 823–828 (Academic Press, Oxford, 2009). doi:10.1016/B978-008045046-9.01352-8.

83. annurev-biochem-061516-045037.pdf.

84. Pahwa, R., Goyal, A. & Jialal, I. Chronic Inflammation. in *StatPearls* (StatPearls Publishing, Treasure Island (FL), 2024).

85. Rossignol, D. A. & Frye, R. E. A review of research trends in physiological abnormalities in autism spectrum disorders: immune dysregulation, inflammation, oxidative stress, mitochondrial dysfunction and environmental toxicant exposures. *Mol. Psychiatry* **17**, 389–401 (2012).

86. Madra, M., Ringel, R. & Margolis, K. G. Gastrointestinal Issues and Autism Spectrum Disorder. *Psychiatr. Clin. North Am.* **44**, 69–81 (2021).

87. Han, V. X., Patel, S., Jones, H. F. & Dale, R. C. Maternal immune activation and neuroinflammation in human neurodevelopmental disorders. *Nat. Rev. Neurol.* **17**, 564–579 (2021).

88. Xie, J., Van Hoecke, L. & Vandenbroucke, R. E. The Impact of Systemic Inflammation on Alzheimer's Disease Pathology. *Front. Immunol.* **12**, 796867 (2022).

89. Rose, S. *et al.* Clinical and Molecular Characteristics of Mitochondrial Dysfunction in Autism Spectrum Disorder. *Mol. Diagn. Ther.* **22**, 571–593 (2018).

90. Mou, Y. *et al.* Gut Microbiota Interact With the Brain Through Systemic Chronic Inflammation: Implications on Neuroinflammation, Neurodegeneration, and Aging. *Front. Immunol.* **13**, 796288 (2022).

91. Than, U. T. T. *et al.* Inflammatory mediators drive neuroinflammation in autism spectrum disorder and cerebral palsy. *Sci. Rep.* **13**, 22587 (2023).

92. Sies, H. Oxidative stress: a concept in redox biology and medicine. *Redox Biol*. **4**, 180–183 (2015).

93. Kerr, J. S. *et al*. Mitophagy and Alzheimer's disease: cellular and molecular mechanisms. *Trends Neurosci*. **40**, 151–166 (2017).